Allosteric Regulation of BK Channel Gating by Ca^{2+} and Mg^{2+} through a Nonselective, Low Affinity Divalent Cation Site

X. Zhang,[1] C.R. Solaro,[1] and C.J. Lingle[1,2]

[1]Department of Anesthesiology, and [2]Department of Anatomy and Neurobiology, Washington University School of Medicine, St. Louis, MO 63110

ABSTRACT The ability of membrane voltage to activate high conductance, calcium-activated (BK-type) K^+ channels is enhanced by cytosolic calcium (Ca^{2+}). Activation is sensitive to a range of [Ca^{2+}] that spans over four orders of magnitude. Here, we examine the activation of BK channels resulting from expression of cloned mouse *Slo1* α subunits at [Ca^{2+}] and [Mg^{2+}] up to 100 mM. The half-activation voltage ($V_{0.5}$) is steeply dependent on [Ca^{2+}] in the micromolar range, but shows a tendency towards saturation over the range of 60–300 μM Ca^{2+}. As [Ca^{2+}] is increased to millimolar levels, the $V_{0.5}$ is strongly shifted again to more negative potentials. When channels are activated by 300 μM Ca^{2+}, further addition of either mM Ca^{2+} or mM Mg^{2+} produces similar negative shifts in steady-state activation. Millimolar Mg^{2+} also produces shifts of similar magnitude in the complete absence of Ca^{2+}. The ability of millimolar concentrations of divalent cations to shift activation is primarily correlated with a slowing of BK current deactivation. At voltages where millimolar elevations in [Ca^{2+}] increase activation rates, addition of 10 mM Mg^{2+} to 0 Ca^{2+} produces little effect on activation time course, while markedly slowing deactivation. This suggests that Mg^{2+} does not participate in Ca^{2+}-dependent steps that influence current activation rate. We conclude that millimolar Mg^{2+} and Ca^{2+} concentrations interact with low affinity, relatively nonselective divalent cation binding sites that are distinct from higher affinity, Ca^{2+}-selective binding sites that increase current activation rates. A symmetrical model with four independent higher affinity Ca^{2+} binding steps, four voltage sensors, and four independent lower affinity Ca^{2+}/Mg^{2+} binding steps describes well the behavior of G-V curves over a range of Ca^{2+} and Mg^{2+}. The ability of a broad range of [Ca^{2+}] to produce shifts in activation of *Slo1* conductance can, therefore, be accounted for by multiple types of divalent cation binding sites.

KEY WORDS: K^+ channels • Ca^{2+}- and voltage-gated K^+ channels • *Slo1* channels • stochastic models • channel kinetics

INTRODUCTION

Most ion channels open in response to a change in a single, primary physiological parameter. In contrast, activation of Ca^{2+}- and voltage-dependent large conductance Ca^{2+}-activated K^+ (BK)* channels is complicated by the fact that two parameters govern channel opening. Membrane depolarization and binding of Ca^{2+} ions interact in some way to bring about an increase in channel open probability. The dependence on Ca^{2+} is particularly remarkable in that the ability of voltage to open BK channels can be shifted by over four log orders of [Ca^{2+}] (Moczydlowski and Latorre, 1983; Meera et al., 1996; Cox et al., 1997a; Cui et al., 1997). Although the voltage dependence of BK channel gating is thought to arise from a mechanism involving voltage-sensing residues in the S4 segment (Diaz et al., 1998; Horrigan et al., 1999; Horrigan and Aldrich, 1999; Cui and Aldrich, 2000), which is similar to the voltage-dependent K^+ channel family, the precise mechanism by which Ca^{2+} exerts its effects remain unknown. Some of the effects of Ca^{2+} may be mediated by interaction of Ca^{2+} with a patch of negatively charged residues, termed the "Ca^{2+} bowl," located just before the S10 hydrophobic segment near the COOH terminus of the *Slo* α subunit (Schreiber and Salkoff, 1997; Schreiber et al., 1999). Residues just upstream of the Ca^{2+} bowl may also participate in defining the Ca^{2+}-regulatory domain (Braun and Sy, 2001). However, how this Ca^{2+}-sensing domain may mediate its effects remains unknown. Moreover, there are several studies that indicate that Ca^{2+} and/or other divalent cations may also allosterically modulate BK gating (Golowasch et al., 1986; Oberhauser et al., 1988; Solaro et al., 1995; Shi and Cui, 2001a).

The relationship between $V_{0.5}$ and cytosolic Ca^{2+} has provided a convenient descriptive tool to evaluate the Ca^{2+} dependence of activation of BK current, an approach first employed by Moczydlowski and Latorre (1983). In this landmark paper (Moczydlowski and

Address correspondence to Chris Lingle, Department of Anesthesiology, Washington University School of Medicine, Box 8054, St. Louis, MO 63110. Fax: (314) 362-8571; E-mail: clingle@morpheus.wustl.edu

*Abbreviations used in this paper: BK, large conductance Ca^{2+}-activated K^+ channel; NMG, *N*-methyl glucamine; P_o, open probability.

Latorre, 1983), the probability of being open of single skeletal muscle BK channels as a function of Ca^{2+} and voltage was examined in bilayers. Over $[Ca^{2+}]$ from near 1 μM to almost 10 mM, the $V_{0.5}$ varied as an essentially linear function of pCa, leading them to propose that Ca^{2+} binding, per se, is the voltage-dependent step in BK channel activation. More recently, a number of labs have investigated the Ca^{2+} dependence of activation of cloned α subunits encoding BK-type channels using primarily macroscopic current measurements (Wei et al., 1994; Meera et al., 1996; Cox et al., 1997a) and found that the relationship between $V_{0.5}$ and pCa may not be quite so simple. Most notably, over a range of $[Ca^{2+}]$ from near 0.5 nM to ~50 nM, currents resulting from expression of cloned subunits appear to be fully activated with sufficiently high voltage, but in a Ca^{2+}-independent fashion (Cui et al., 1997; Horrigan et al., 1999). Furthermore, the G-V curve for activation and the time constant of current activation remains relatively insensitive to Ca^{2+} over the range of 5 to ~50 nM Ca^{2+} (Cui et al., 1997). However, over the range of Ca^{2+} from ~0.5 to ~100 μM, $V_{0.5}$ shifts to more negative potentials, before beginning to exhibit some saturation from ~100 μM to 1 mM (Wei et al., 1994; Cox et al., 1997a; Cui et al., 1997). The extent of this saturation appears to exhibit some variability among work from different labs or even within the same lab (Wei et al., 1994; Meera et al., 1996; Cox et al., 1997a; Cui et al., 1997; Wallner et al., 1999), although the reasons for this remain unclear. To account for the Ca^{2+} dependence of the shift in G-V curves, activation models involving separate and independent Ca^{2+} binding and voltage-dependent steps have proven useful (Cox et al., 1997a; Horrigan et al., 1999; Rothberg and Magleby, 1999; Cox and Aldrich, 2000; Cui and Aldrich, 2000). However, an additional feature of activation of cloned BK channels (Wei et al., 1994; Solaro et al., 1995; Meera et al., 1996) and native BK channels (Moczydlowski and Latorre, 1983) is that, as Ca^{2+} is raised above 1 mM, there appears to be an additional shift in the $V_{0.5}$, which is inconsistent with most current models of Ca^{2+} dependence of BK activation. As yet, these effects of mM concentrations of Ca^{2+} are not understood.

In addition to its ability to shift gating over such a broad concentration range, one of the remarkable characteristics of the ability of Ca^{2+} to promote activation of BK channels is its high selectivity over other divalent cations. In particular, although both Sr^{2+} and Mn^{2+} can activate BK channels in the absence of Ca^{2+}, they are relatively ineffective compared with Ca^{2+} (Oberhauser et al., 1988). Other divalent cations such as Mg^{2+}, Ni^{2+}, and Pb^{2+} are ineffective at opening BK channels effects (Oberhauser et al., 1988), although Mg^{2+} and Ni^{2+}, but not Pb^{2+}, enhance activation of channels already activated by Ca^{2+} (Golowasch et al., 1986; Oberhauser et al., 1988). The enhancement of activation involves an increase in the apparent Hill coefficient for activation by Ca^{2+} (Golowasch et al., 1986; Oberhauser et al., 1988). Together, these earlier results raise the possibility that multiple kinds of divalent cation binding sites may regulate BK channel gating, thereby perhaps accounting, in part, for the ability of Ca^{2+} to modulate BK gating over such a wide range of $[Ca^{2+}]$.

To address these issues, we have examined effects of millimolar $[Ca^{2+}]$ on the gating of currents resulting from expression of the m*Slo1* α subunit and compared this with the ability of Mg^{2+} to alter currents resulting from activation by various concentrations of Ca^{2+}. We show that the enhancement in BK current activation by $[Ca^{2+}]$ of 1 mM and greater or by millimolar Mg^{2+} added to Ca^{2+}-containing solutions can be accounted for by a low affinity, divalent cation binding site that affects channel activation in a way quite distinct from the effects of μM Ca^{2+}. The enhancement by Mg^{2+} occurs in the complete absence of Ca^{2+}, which indicates that Mg^{2+} does not modify Ca^{2+} binding steps. Furthermore, Mg^{2+} does not substitute for Ca^{2+} at the high affinity Ca^{2+} binding sites. The shifts in gating produced by millimolar Mg^{2+} do not involve increases in current activation rates, but do involve a slowing of the return to closed states. Thus, qualitatively, millimolar concentrations of divalents appear to enhance BK activation by affecting the closed-to-open channel equilibrium without direct effects on Ca^{2+} affinities. A similar conclusion has also been drawn in the companion paper by Shi and Cui (2001b). To account for these observations, we propose a simple extension of a specific two-tiered 50-state activation model proposed by Cox and Aldrich (2000). We postulate that, in addition to the regulation of *Slo1* gating by four independent high affinity Ca^{2+} binding steps and independent movement of four voltage sensors, binding of Mg^{2+} also allosterically regulates *Slo1* opening independent of Ca^{2+} binding and voltage-sensor movement. Such a model accurately reproduces the behavior of G-V curves for Ca^{2+} from 0 to 100 mM, with Mg^{2+} from 1 to 100 mM. The analysis suggests that, although Mg^{2+} and Ca^{2+} appear to have similar effects at millimolar concentrations, the affinities of Ca^{2+} to the low affinity sites on open and closed channels are about seven- to eightfold greater than the affinities of Mg^{2+}, which indicates that under physiological conditions, the low affinity sites may participate in the regulation of BK channel gating. The success of this model is improved by taking into account the proposal that millimolar Mg^{2+} acts not only to promote activation through the low affinity site, but also to inhibit Ca^{2+} binding at the high affinity Ca^{2+} binding site (see Shi and Cui, 2001b, in this issue).

MATERIALS AND METHODS

Oocyte Removal and Culture

Mature stage IV *Xenopus laevis* oocytes were prepared for injection as described in previous work (Wei et al., 1994; Xia et al., 1999; Lingle et al., 2001; Zeng et al., 2001).

Constructs

The *mSlo1* (Butler et al., 1993) construct used in initial experiments was provided by L. Salkoff (Washington University) and is identical to that used in earlier work (Wei et al., 1994). In more recent experiments, *mSlo1* was placed in an alternative vector (Xia et al., 1999). No differences in physiological properties have been observed between the two constructs.

Recording Pipettes

Patch-clamp recording pipettes were made by pulling borosilicate capillary tubes (Drummond Microcaps; 100 μl) to a tip diameter of ~1 μM. Pipette resistances (R_p) measured in recording salines ranged from 1.5 to 10 MΩ for single-channel recordings and from 1.5 to 3 MΩ for macroscopic currents. Because of the large currents obtained with *Slo1* expression, the series resistance (R_s) associated with the pipette may result in nominal voltage values that are different from the true applied voltage. In most experiments, we only used patches in which the maximal current at +100 mV was ~5 nA or less. Although larger currents were typically associated with pipettes of smaller R_p, in the worst cases currents may still result in a voltage errors of 5–15 mV. However, close examination of the G-V curves from individual patches used to generate the averaged G-V curves of Fig. 2 B does not reveal any systematic correlation of $V_{0.5}$ with current density at any [Ca^{2+}]. All voltage values reported here have been uncorrected for possible series resistance errors.

Pipette tips and shanks were coated with a silicone elastomer (Sylgard 184; Dow Chemical Corp.) and firepolished. A pipette was then filled with an appropriate recording saline and placed over a chloridized silver wire attached to the recording headstage. For some experiments, the reference electrode was a silver chloride pellet immersed in 3M KCl which, in turn, was connected to the recording dish by a KCl-agar bridge (4% agar in 3M KCl). In other experiments, a silver chloride pellet alone was used.

Electrophysiology

Calcium- and voltage-activated potassium channel currents were recorded in the inside-out configuration according to standard procedures (Hamill et al., 1981) using an Axopatch 1C amplifier (Axon Instruments, Inc.) with a 50-GΩ feedback resistor and the Clampex program from the pClamp software package (Axon Instruments, Inc.). Currents were recorded in patches pulled from oocytes 1–9 d after injection with cRNAs. Patches used to construct conductance/voltage relationships typically contained large numbers (>50) of *Slo1* channels. The room temperature for these experiments was ~23°C.

Gigaohm seals were formed on oocytes bathed in normal frog Ringer's solution ([in mM] 115 NaCl, 2.5 KCl, 1.8 $CaCl_2$, and 10 HEPES, pH 7.4) and, after excision, were transferred to test solutions containing calcium. Pipette/extracellular solution was (in mM) 140 potassium methanesulfonate, 20 KOH, 10 HEPES, and 2 $MgCl_2$, pH 7.0. Test solutions bathing the cytoplasmic face of the patch membrane contained (in mM): 140 potassium methanesulfonate, 20 KOH, and 10 HEPES, pH 7.0 and one of the following: 5 EGTA, for nominally 0 Ca^{2+} and for 1 μM Ca^{2+} solutions; 5 HEDTA for 4 and 10 μM Ca^{2+}; or no added Ca^{2+} buffer for solutions of 30 μM Ca^{2+} and higher. In earlier experiments (Solaro et al., 1995), solutions were calibrated (93-20 Ca^{2+} sensor; Orion) against chloride-based solutions in which free Ca^{2+} was determined using the EGTAETC computer program (E. McCleskey, Vollum Institute). Solutions for more recent experiments were calibrated with commercial Ca^{2+} calibration solutions (WPI). Comparison of our chloride-based solutions with the commercial standards yielded similar estimates of Ca^{2+} concentrations.

Mixed Ca^{2+}/Mg^{2+} solutions were prepared as follows. A 2-M $MgCl_2$ stock solution (crystalline $MgCl_2$; Puratronic, 99.999%; Alfa-Aesar; <0.001% Ca^{2+} contamination) was prepared with Chelex (Sigma-Aldrich)-treated distilled H_2O. Based on the manufacturer's estimate of the Ca^{2+} contamination in the original $MgCl_2$ material, the 2- M $MgCl_2$ stock should have contained <20 μM Ca^{2+}, which would contribute negligible amounts of Ca^{2+} at the dilutions we have used. The concentration of Ca^{2+} in Chelex-treated KCl-based solutions was below the limits of Ca^{2+} electrode resolution, but yielded G-V curves from *Slo1* channels similar to those obtained with solutions with 0 Ca^{2+}, 5 mM EGTA. For K^+-MES–based solutions, we were unable to reduce background Ca^{2+} with Chelex below 1 μM. Without Chelex treatment, electrode readings indicated that K^+-MES solutions with no added Ca^{2+} typically contained 10–15 μM free Ca^{2+}. For unbuffered Ca^{2+} solutions (K^+-MES) of 30 μM Ca^{2+} and higher, Mg^{2+} was simply added to make the appropriate concentration from the 2-M $MgCl_2$ stock solution. For additions of Mg^{2+} to solutions containing 0 μM Ca^{2+}, 5 mM EGTA, we simply added $MgCl_2$ directly to result in the nominal concentrations of Mg^{2+} indicated in the results.

Based on published stability constants for EGTA, Mg^{2+}, Ca^{2+}, and H^+, we estimated the consequences of this addition using EQCALWIN (Biosoft). If we assume a worst case maximal contaminant [Ca^{2+}] from all sources of 30 μM (K^+-MES stock, $MgCl_2$ stock, deionized water), with 5 mM EGTA and 100 mM $MgCl_2$, the calculated free Ca^{2+} and free Mg^{2+} is 9.6 nM and 97 mM, respectively. At 10 mM nominal $MgCl_2$, the calculated free Ca^{2+} and free Mg^{2+} is 2.71 nM and 8.8 mM, respectively. With no added $MgCl_2$, the calculated free Ca^{2+} is 2.0 nM. *Slo1* currents have been shown to be unaffected by changes in free Ca^{2+} over the range of 0.5–50 nM (Cui et al., 1997). Thus, the effects observed with 0 Mg^{2+} are unlikely to result from contamination by Ca^{2+}. In reporting the results, we have used the nominal values for free [Mg^{2+}], corresponding to a maximum error of ~15% in the actual [Mg^{2+}] at the lower concentrations of Mg^{2+} (1 mM). These errors do not apply to the unbuffered solutions.

In one set of experiments, unbuffered 0-, 4-, and 10-μM Ca^{2+} solutions were prepared using KCl (rather then K-MES). For preparation of these solutions, a 1-M KCl stock solution was stirred with Chelex for 2–3 h. Finally, after calibration of the Ca^{2+}-sensitive electrode, aliquots of a 10-mM $CaCl_2$ solution were added until the desired electrode reading was achieved. $MgCl_2$ was subsequently added by dilution from the 2-M Mg^{2+} stock solution. The properties of a 0-Ca^{2+} solution prepared in this way and compared with the 0-Ca^{2+}, 5-mM EGTA solutions (as described in *Electrophysiology*) indicated that the background Ca^{2+} was in the low nanomolar range. Despite the fact after addition of $MgCl_2$ such a 10-mM Mg^{2+} solution should contain <1 μM contaminant Ca^{2+}, we were still concerned that the effects of addition of Mg^{2+} to solutions with low [Ca^{2+}] might result from addition of contaminant Ca^{2+}. However, RESULTS indicate that some aspects of the kinetic alterations resulting from addition of Mg^{2+} are inconsistent with the possibility that the effects are being produced by additional Ca^{2+}. In patches, in which 0-, 4-, and 10-μM unbuffered Ca^{2+} solutions were examined, control solutions with buffered 0, 4 and 10 μM Ca^{2+} were also examined to ensure that solutions with similar concentrations yielded similar results. The similarity of the G-V curves obtained with both buffered and unbuffered Ca^{2+} suggests that intrinsic Ca^{2+} buffering associated with components of the excised

patch are minimal. EQCALWIN also was used to calculate expected free Mg^{2+} and free Ca^{2+} in ATP-containing solutions using published stability constants (Martell and Smith, 1975).

For these experiments, we frequently used divalent cation concentrations up to 100 mM Mg^{2+} or Ca^{2+}. This resulted in solutions with elevated osmolarity compared with the usual solutions containing 1 mM or lower Ca^{2+}. Such solutions also contain elevated Cl^-. We were concerned that these factors might, therefore, influence the conductance-voltage curves, which is independent of the divalent cation concentrations. Several control experiments were done. First, the effect of adding Mg^{2+} as either $MgCl_2$ or $MgSO_4$ was compared and found to be identical. Second, we prepared 300-μM Ca^{2+} solutions with added 150 mM *N*-methylglucamine (NMG) and found that for a set of four patches, G-V curves were identical for 300 μM Ca^{2+} either with ($V_{0.5}$ = −23.1 ± 3.2 mV) or without ($V_{0.5}$ = −20.5 ± 5.6 mV) NMG. Thus, the increase in osmolarity and ionic strength resulting from the addition of NMG does not have a substantial effect on G-V curves activated by 300 μM Ca^{2+}. Similarly, current activation time constants were identical in the two cases. However, with 150 mM NMG, there was a weak voltage-dependent reduction in outward current, perhaps reflecting a weak, rapid blocking effect of NMG on the channel.

Solution Exchange

Solution exchange and drug applications were accomplished with a multibarrel solution delivery system as used previously described (Wei et al., 1994; Herrington et al., 1995; Zeng et al., 2001). In this system, six to seven polyethylene 10 (PE10) tubes were packed into the end of a glass tube that was tapered at one end to an ∼ 50-μm open tip. Solution flowed through one line at all times, and complete solution exchange at the patch membrane required ∼100 ms.

Data Analysis

Analysis of current recordings was done either with Clampfit (Axon Instruments, Inc.) or with programs written in this laboratory. For analysis of patches with one or two channels, leakage subtraction was accomplished by subtracting from the experimental records either an average of records in which no channels opened (either by chance or during perfusion with zero Ca^{2+} saline) or by subtracting an idealized sweep (using a sweep obtained in 0 Ca^{2+} as a template) generated to match the experimental leak current. Ensemble averages of BK channel probability of being open (P_o) were generated from idealized single-channel current records using a 50% threshold detection algorithm. The single-channel open level was given a value of one and the single-channel closing level was given a value of zero. When the number of channels in the patch (N) is known, average P_o can be calculated directly by averaging the idealized records and dividing the average by N. Currents or extracted data were fit using a Levenberg-Marquardt search algorithm to obtain nonlinear least-squares estimates of function parameters.

G-V curves were constructed primarily from tail currents measured 100–200 μs after repolarization and, in some cases, from the peak current measured at a given voltage. Typically, the absolute value of maximal conductance was similar at Ca^{2+} concentrations between 4 and 300 μM, whereas at lower or higher Ca^{2+}, the observed value for maximal conductance was smaller. In such cases, conductance estimates were normalized to the maximal value observed over the range of 10–300 μM Ca^{2+}. Individual G-V curves were typically fit with a standard Boltzmann function of the following form:

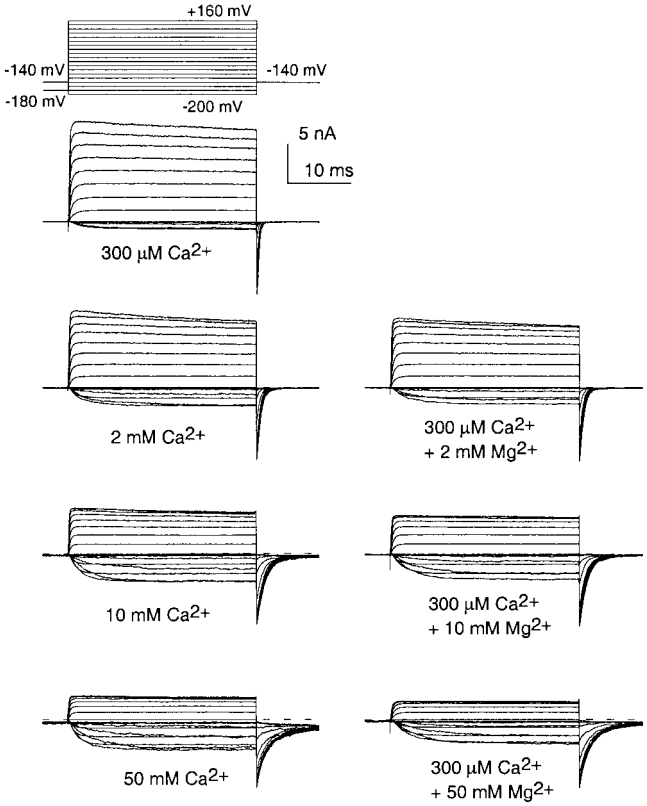

FIGURE 1. Similar enhancement of *Slo1* current activation by high concentrations of either Ca^{2+} and Mg^{2+}. Each family of traces shows currents from the same inside-out patch from a *Xenopus* oocyte, expressing *mSlo1* α subunits. Currents were activated by the voltage protocol shown on the top left with the indicated divalent cation concentrations applied to the cytosolic face of the patch. On the left, traces were obtained with 300 μM Ca^{2+}, 2 mM Ca^{2+}, 10 mM Ca^{2+} and 50 mM Ca^{2+} from top to bottom. On the right, each family of traces was obtained with 300 μM Ca^{2+} but with added 2, 10, and 50 mM Mg^{2+} from top to bottom. Tail currents were recorded at −140 mV. For solutions containing 10 and 50 mM divalent, the potential before the activation steps (−200 to +160 mV) was −180 mV, and −140 in other cases. Note the strong slowing of deactivation with either Ca^{2+} and Mg^{2+}, the similar activation of current with additions of mM Ca^{2+} or Mg^{2+}, and the strong block of current at positive activation potential at higher divalent concentrations.

$$G(V) = \frac{G_{max}}{1 + \exp\frac{-(V - V_{0.5})}{k}}, \quad (1)$$

where G_{max} is the fitted value for maximal conductance, $V_{0.5}$ is the voltage of half maximal activation of conductance, and k is the term for the voltage dependence of activation in units of mV.

Fitting of G-V curves to equations defined by particular kinetic models was done with our own software in which a Levenberg-Marquardt optimization routine was used to perform a nonlinear least-squares minimization. To confirm the validity of the implementation of the fitting routine, for any given set of parameter values defined by a given function (e.g., see Eq. 4), the curves defined by the function were also checked with an implementation of the function in Mathcad (Mathsoft).

RESULTS

Millimolar Concentrations of Mg^{2+} and Ca^{2+} Produce Similar Shifts in the Voltage of Half Activation ($V_{0.5}$).

Fig. 1 shows currents from an excised inside-out patch expressing *mSlo1* α subunits. On the left, currents were activated with 300 μM, 2 mM, 10 mM, and 50 mM Ca^{2+}. On the right, currents were activated with 300 μM Ca^{2+} with 2, 10, and 50 mM Mg^{2+}. Qualitatively, it can be seen that the effect produced by increases in [Ca^{2+}] above 300 μM appear to be mimicked by comparable increases in [Mg^{2+}].

Fig. 2 A shows corresponding conductance-voltage relationships (G-Vs) determined from measurements of tail current for the four Ca^{2+} concentrations illustrated in Fig. 1, whereas Fig. 2 B shows the effects of additions of Mg^{2+} to current activated by 300 μM Ca^{2+}. In Fig. 2 C, G-V curves resulting from 300 μM Ca^{2+}, 10 mM Ca^{2+} and 300 μM Ca^{2+} plus 10 mM Mg^{2+} are directly compared. It can be seen that once current is activated by 300 μM Ca^{2+}, additions of either Ca^{2+} or Mg^{2+} are relatively comparable in their ability to shift G-V curves.

High concentrations of Ca^{2+} also block *Slo1* currents. This block is indicated by the voltage-dependent reduction of current at the most positive activation voltages in the presence of 10 and 50 mM Ca^{2+} (Fig. 1). Mg^{2+} also produces a similar voltage-dependent reduction of peak current. This reduction in peak macroscopic conductance is almost entirely mediated by fast channel block (Vergara and Latorre, 1983; Ferguson, 1991), which can be seen in the reduction of single-channel current amplitude with high [Ca^{2+}] (data not shown for Ca^{2+} [unpublished data], but see results in Fig. 3 with Mg^{2+} below).

For a set of patches, the relationship between conductance and activation voltage was determined over Ca^{2+} concentrations from 1 μM to 100 mM (Fig. 2 D). Similarly, in parallel experiments, the effect of Mg^{2+} from 1 mM to 100 mM on currents activated by 300 μM Ca^{2+} was determined (Fig. 2 E). G-V curves were fit with a single Boltzmann (Eq. 1) and the relationship between $V_{0.5}$ and pCa for a large number of patches is plotted in Fig. 2 F. There are two key features. As [Ca^{2+}] is raised to 300 μM, the rate of change in the voltage of half activation appears to slow similar to previous observations (Wei et al., 1994; Cox et al., 1997b; Cui et al., 1997). However, at 10 mM Ca^{2+}, activation is shifted dramatically to more negative potentials by an additional ~40–50 mV.

Activation of Slo1 by Ca^{2+} Is Potentiated by Internal Mg^{2+}

The additional leftward shift of activation caused by mM concentrations of Ca^{2+} coupled with the inflection observed in the $V_{0.5}$ versus pCa plot raise the possibility that Ca^{2+} is shifting activation of *Slo1* channels through a process distinct from the Ca^{2+}-dependent activation steps that occur at lower [Ca^{2+}]. The fact that, in the presence of 300 μM Ca^{2+}, millimolar Mg^{2+} and Ca^{2+} are similarly effective at shifting the $V_{0.5}$ also supports the idea that effects of mM divalents may involve a different site and mechanism than the gating effects produced by micromolar Ca^{2+}.

It has been shown previously that, in the presence of micromolar Ca^{2+}, millimolar concentrations of internal Mg^{2+} can potentiate activation of BK channels recorded from rat skeletal muscle transverse tubule membranes (Golowasch et al., 1986; Oberhauser et al., 1988). Because Mg^{2+} produces minimal channel activation in the absence of Ca^{2+}, it has been proposed that Mg^{2+} is a positive allosteric modulator of BK channel activity. 400 μM nickel in the presence of 1 μM Ca^{2+} is also able to shift the $V_{0.5}$ of this channel by ~44 mV negative to that measured with 1 μM Ca^{2+} alone (Oberhauser et al., 1988). Like Mg^{2+}, Ni^{2+} alone is relatively ineffective at activating BK channels. This suggests that some divalent cations may influence BK gating at a secondary allosteric site. The leftward shift of $V_{0.5}$ measured for *Slo1* with 10 mM Ca^{2+}, then, could be caused by an association of Ca^{2+} itself with this relatively nonselective site. The experiments presented below address this hypothesis.

Mg^{2+}-induced Shifts in the Single-channel Probability of Being Open Are Similar to Shifts in Macroscopic Currents

Fig. 3 shows that a leftward shift of activation by 10 mM Mg^{2+} is also evident at the single-channel level. For these experiments, inside-out patches containing one or two channels were stepped repeatedly to particular test potentials. Fig. 3 A shows sample records from a patch containing two channels in which activation is compared at both +60 and −60 mV in the presence of either 300 μM Ca^{2+} or 300 μM Ca^{2+} + 10 mM Mg^{2+}. For a given condition, the probability of channels being open (P_o) was measured for each sweep and an average P_o was generated for a set of sweeps. Fig. 3 B summarizes the average P_o determined over a range of voltages from the experiment in Fig. 3 A. Superimposed solid lines are fitted single Boltzmann relations. The plot shows that 10 mM Mg^{2+} is able to shift activation, as measured by P_o, leftward by ~50 mV. This is similar to the magnitude of the shift measured for macroscopic currents. Both with and without Mg^{2+}, the saturating P_o is similar and approaches ~90%.

Fig. 3 C plots P_o estimates as a function of test potential for an experiment similar to that of Fig. 3 A in which channels were activated by either 100 μM Ca^{2+}, 100 μM Ca^{2+} plus 10 mM $MgCl_2$, 10 mM Ca^{2+} or 10 mM Ca^{2+} plus 10 mM Mg^{2+}. The P_o-V relationships for the latter three solutions are all quite similar. This indicates that, in the presence of 100 μM Ca^{2+}, addition of

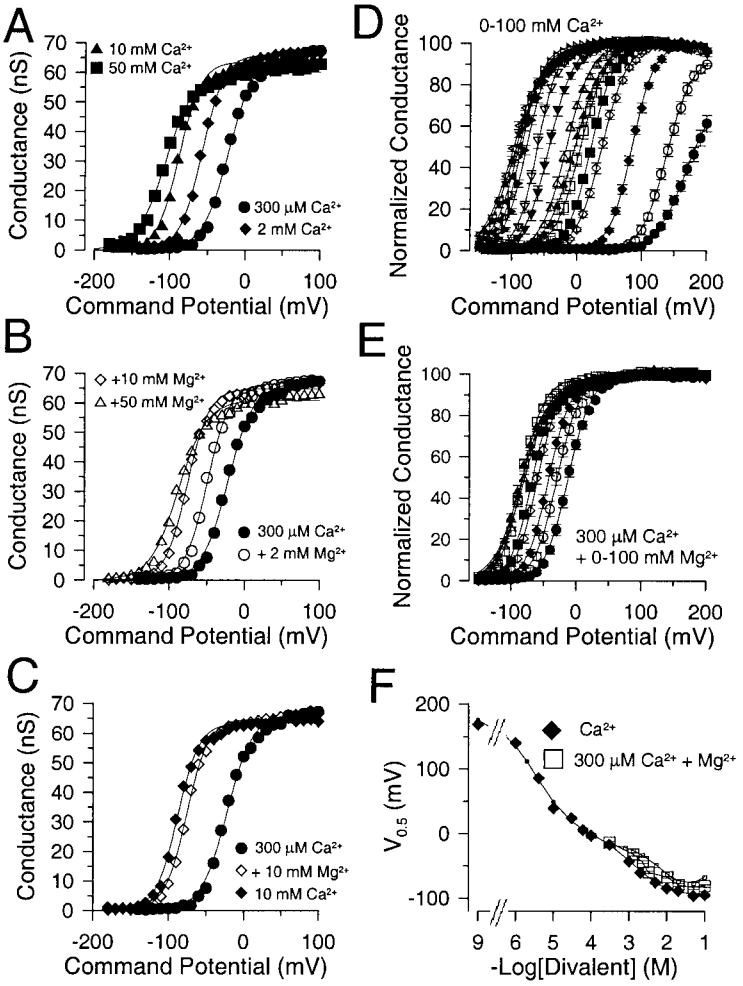

FIGURE 2. High concentrations of Ca^{2+} and Mg^{2+} are similarly effective at shifting current activation. In A, G-V curves were generated from tail currents obtained with 300 μM, 2 mM, 10 mM and 50 mM Ca^{2+} (patch in Fig. 1). Solid lines are fits of Eq. 1, with values for $V_{0.5}$ of −21.5 ± 1.0 mV (k = 17.1 mV), −57.1 ± 0.7 mV (k = 14.6 mV), −87.5 ± 0.7 mV (k = 14.4 mV) and −104.5 ± 1.1 mV (k = 19.0 mV), for 300 μM–50 mM Ca^{2+}, respectively. In B, G-V curves from the same patch as in A are shown for currents obtained with 300 μM Ca^{2+}, and 300 μM Ca^{2+} with either 2, 10, or 50 mM added Mg^{2+}. Values for $V_{0.5}$ for 2, 10, and 50 mM Mg^{2+} containing solutions were as follows: −48.7 ± 1.0 mV (k = 14.8 mV), −75.5 ± 0.8 mV (k = 14.5 mV), and −87.4 ± 1.1 mV (k = 18.7 mV), respectively. In C, G-V curves are shown for 300 μM Ca^{2+}, 20 mM Ca^{2+}, and 300 μM Ca^{2+} + 20 mM Mg^{2+}. In D, the mean conductance measured as a function of voltage is displayed for a set of patches over a range of Ca^{2+} concentrations from 0 to 100 mM. Solid lines are fits of Eq. 1. For 0 Ca^{2+} (●), $V_{0.5}$ = 168.5 ± 2.2 mV, k = 22.4 ± 1.0 mV; for 1 μM Ca^{2+} (○), $V_{0.5}$ = 136.89 ± 0.9 mV, k = 18.8 ± 0.7 mV; for 4 μM (◆), $V_{0.5}$ = 85.2 ± 0.6 mV, k = 16.9 ± 0.5 mV; for 10 μM (◇), $V_{0.5}$ = 39.0 ± 0.5 mV, k = 19.1 ± 0.5 mV; for 30 μM (■), $V_{0.5}$ = 22.4 ± 0.5 mV, k = 17.9 ± 0.4 mV; for 60 μM (□), $V_{0.5}$ = 5.8 ± 0.8 mV, k = 19.3 ± 0.5 mV; for 100 μM (▲), $V_{0.5}$ = −2.4 ± 0.7 mV, k = 21.2 ± 0.5 mV; for 300 μM (△), $V_{0.5}$ = −15.9 ± 0.6 mV, k = 18.9 ± 0.5 mV; for 1 mM (▼), $V_{0.5}$ = −42.4 ± 0.6, k = 18.4 ± 0.5 mV; for 2 mM (▽), $V_{0.5}$ = −60.5 ± 0.6 mV, k = 15.6 ± 0.5 mV; for 5 mM (▶), $V_{0.5}$ = −77.6 ± 0.8 mV, k = 16.9 ± 0.7 mV; for 10 mM (▷), $V_{0.5}$ = −85.2 ± 0.8 mV, k = 16.5 ± 0.7 mV; for 20 mM (◀), $V_{0.5}$ = −89.3 ± 0.8 mV, k = 19.0 ± 0.7 mV; for 50 mM (◁), $V_{0.5}$ = −97.9 + 1.1 mV, k = 22.2 ± 0.9 mV; and for 100 mM (★), $V_{0.5}$ = −93.5 ± 0.9 mV, k = 22.5 ± 0.8 mV. Each point represents the mean with SD of from 4 to 12 patches. In E, G-V curves were generated from a set of patches (mean and SD for 4–19 patches) with 300 μM Ca^{2+} with various Mg^{2+} concentrations. Solid lines are fits of Eq. 1. For 300 μM (●), $V_{0.5}$ = −11.6 ± 0.5 and k = 17.8 ± 0.5 mV; with 1 mM Mg^{2+} (○), $V_{0.5}$ = −28.5 ± 0.7 mV, k = 17.4 ± 0.6 mV; with 2 mM Mg^{2+} (◆), $V_{0.5}$ = −41.4 ± 0.6 mV, k = 17.1 ± 0.5 mV; with 5 mM Mg^{2+} (◇), $V_{0.5}$ = −58.4 ± 0.6 mV, k = 16.9 ± 0.6 mV; with 10 mM Mg^{2+} (■), $V_{0.5}$ = −67.1 ± 0.7 mV, k = 16.5 ± 0.6 mV; with 20 mM Mg^{2+} (□), $V_{0.5}$ = −82.6 ± 0.8 mV, k = 16.8 ± 0.7 mV; with 50 mM Mg^{2+} (▲), $V_{0.5}$ = −82.8 ± 1.4 mV, k = 21.6 ± 1.3 mV; and 100 mM Mg^{2+} (△), $V_{0.5}$ = −79.6 ± 1.3 mV, k = 21.3 ± 1.1 mV. In F, $V_{0.5}$ values measured in D and E are plotted as a function of the indicated divalent cation concentration for either solutions with Ca^{2+} alone (◆) or for 300 μM Ca^{2+} with added Mg^{2+} (□). The 5 mM EGTA, 0 Ca^{2+} solution was plotted as 10^{-9} M. Solid lines with small filled circles (Ca^{2+} alone) and small open squares (300 μM Ca^{2+} plus Δ[Mg^{2+}]) represents expectations derived from a fit of Scheme I (values from Table II, column D) to the G-V curves in Fig. 2 D.

Mg^{2+} is about as effective as an increase in Ca^{2+} at producing leftward shifts in the activation curves. In contrast, the further addition of 10 mM Mg^{2+} to 10 mM Ca^{2+} is ineffective at producing an additional shift. The $V_{0.5}$ estimates measured at the single-channel level in the presence and absence of 10 mM Mg^{2+} are similar to those measured for macroscopic currents.

The Magnitude of the Shift in $V_{0.5}$ Produced by Mg^{2+} Is Not Ca^{2+}-dependent

We next examined the ability of Mg^{2+} to shift G-V curves at lower [Ca^{2+}]. Fig. 4 A gives an example of the effect of 10 mM Mg^{2+} on *Slo1* currents activated in the absence of Ca^{2+}. G-V curves (Fig. 4 B) were generated for a set of patches with 0-μM Ca^{2+} solutions, 0 Ca^{2+}/10 mM Mg^{2+}, and 0 Ca^{2+}/50 mM Mg^{2+}. When 10 mM Mg^{2+} is added to 0-Ca^{2+} solutions, conductance begins to be activated ~50 mV negative to that observed absence of Mg^{2+}, a shift similar to that observed when 10 mM Mg^{2+} is added to a solution with 300 μM Ca^{2+}. It might be argued that this shift results from the addition of contaminant Ca^{2+} in the Mg^{2+} solution. However, as described in the MATERIALS AND METHODS, in the solutions with 0 μM Ca^{2+}/10 mM Mg^{2+}/5 mM EGTA, the free [Ca^{2+}] is unlikely to exceed even 10 nM, a concentration that does not activate BK current. Furthermore, the effects of the addition of Mg^{2+} on current activation time course appear inconsistent with the expected effects of an addition of Ca^{2+}. Although the effects of Ca^{2+} on activation time course are complex at activation

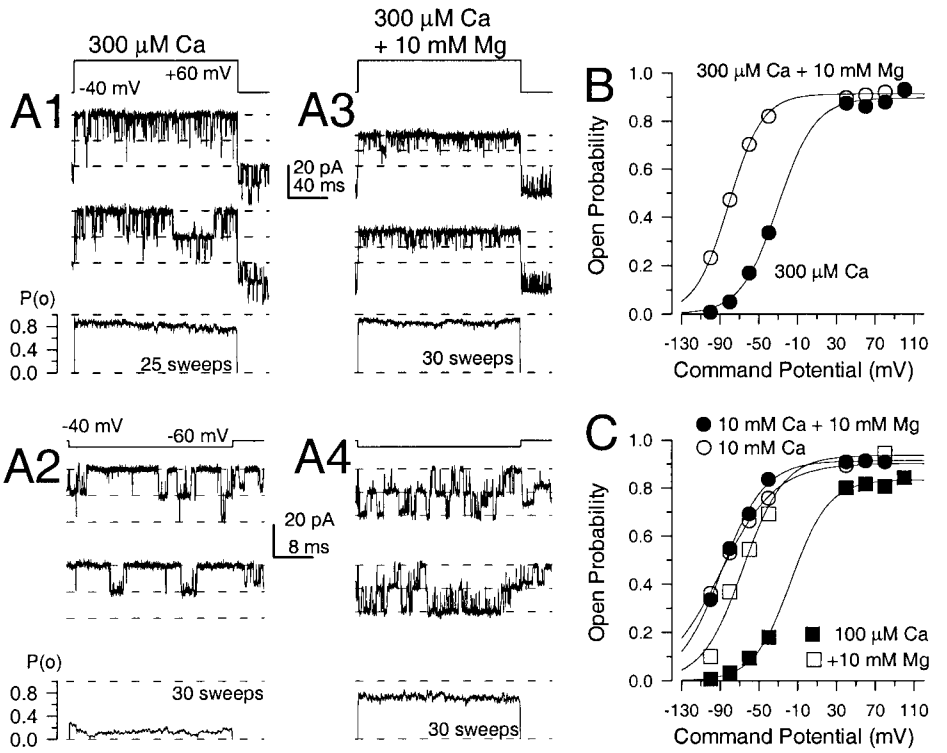

FIGURE 3. Millimolar Mg^{2+} and Ca^{2+} produce similar shifts to more negative potentials in the relationship between open probability and voltage. In A, traces show currents from an inside-out patch containing two BK channels. Patches were held at −40 mV with repeated voltage steps to either +60 mV (A1 and A3), or −60 mV (A2 and A4). On the left (A1 and A2), channels were activated with 300 μM Ca^{2+}, whereas on the right (A3 and A4) channels were activated with 300 μM Ca^{2+} plus 10 mM Mg^{2+}. In each panel, the ensemble average expressed in units of probability of being open (P_o) is plotted at the bottom. At +60 mV, the addition of Mg^{2+} has little effect on P_o, but reduces the single-channel current amplitude. At −60 mV, Mg^{2+} produces a substantial increase in P_o, with only a mild reduction in the single-channel amplitude. In B, P_o estimates obtained from the ensemble averages are plotted as a function of command potential for the patch shown in A. Solid lines are fits of Eq. 1. At 300 μM Ca^{2+}, fitted values with 90% confidence limits were $g_{max} = 0.89 \pm 0.02$, $V_{0.5} = -30.7 \pm 5.1$ mV, and $k = 19.2 \pm 4.4$ mV; for 300 μM Ca^{2+} plus 10 mM Mg^{2+}, $g_{max} = 0.91 \pm 0.01$, $V_{0.5} = -81.0 \pm 1.0$ mV, and $k = 17.9 \pm 1.0$ mV. In C, P_o versus voltage is plotted for a different patch showing that activation by 10 mM Ca^{2+} is similar to that produced by 10 mM Ca^{2+} plus 10 mM Mg^{2+}. Fitted values were as follows: for 100 μM Ca^{2+}, $g_{max} = 0.83 \pm 0.02$, $V_{0.5} = -16.5 \pm 4.9$ mV, and $k = 19.4 \pm 2.7$ mV; for 100 μM Ca^{2+} plus 10 mM Mg^{2+}, $g_{max} = 0.94 \pm 0.11$, $V_{0.5} = -66.2 \pm 8.9$ mV, and $k = 21.3 \pm 8.5$ mV; for 10 mM Ca^{2+}, $g_{max} = 0.91 \pm 0.06$, $V_{0.5} = -89.2 \pm 5.4$ mV, and $k = 25 \pm 6.9$ mV; and for 10 mM Ca^{2+} plus 10 mM Mg^{2+}, $g_{max} = 0.92 \pm 0.04$, $V_{0.5} = -87.7 \pm 3.2$ mV, and $k = 22.6 \pm 3.8$ mV.

potentials above the voltage of half activation of current, 10 mM Mg^{2+} produces little effect on the current activation time course (Fig. 9 E), whereas small increases in [Ca^{2+}] typically increase current activation rates. Thus, the effect of Mg^{2+} appears to differ from what would be expected from the addition of Ca^{2+}. This slowing in activation rate also suggests that the mechanism of Mg^{2+} action is clearly distinct from the changes in gating that occur with lower concentrations of Ca^{2+}.

The ability of Mg^{2+} to shift activation was also examined with solutions containing either 4 or 10 μM free Ca^{2+}. (Fig. 4, D–F). The shift resulting from 10 mM Mg^{2+} in this set of four patches was ~25 mV, less than observed either at 0 or 300 μM Ca^{2+}. An even smaller shift was produced by 10 mM Mg^{2+} with 10 μM Ca^{2+} in the experiments of Shi and Cui (2001b). Given that 10 mM Mg^{2+} appears to produce similar shifts in $V_{0.5}$ at both 0 Ca^{2+} and more elevated Ca^{2+}, the smaller effect at intermediate [Ca^{2+}] seems at first glance unusual. Shi and Cui interpreted this smaller shift as the result of an inhibitory effect of Mg^{2+} on the Ca^{2+} binding site (see Shi and Cui, 2001b, in this issue). Perhaps consistent with this possibility, when Mg^{2+} was added to solutions with either 4 or 10 μM Ca^{2+}, there was a slowing in the current activation time course (Fig. 4, D and F). Such a slowing might result simply from inhibition by Mg^{2+} of Ca^{2+} binding.

The slowing of the activation time course might also be explained by the possibility that Mg^{2+} was shifting channel activation from a condition of very low open probability to approximately half-maximal open probability. For example, in the simple case of a two-state system,

$$C_n \underset{\beta(V)}{\overset{\alpha(V)}{\rightleftharpoons}} O_n$$

where $\tau(V) = 1/(\alpha(V) + \beta(V))$, the slowest $\tau(V)$ is achieved when $\alpha(V) = \beta(V)$. For the effect of Mg^{2+} on *Slo1* currents shown in Fig. 4 D, this possibility seemed unlikely since at 10 μM [Ca^{2+}] and +80 mV, currents should be at least half maximally activated. To verify this directly, the ability of Mg^{2+} to enhance current activation at a given potential was examined in one or two channel patches in which it was possible to directly define the effect of Mg^{2+} on single-channel open probability. Such an experiment shown in Fig. 4 F confirms that the slowing of the activation time course even occurs as the open probability goes from about half maxi-

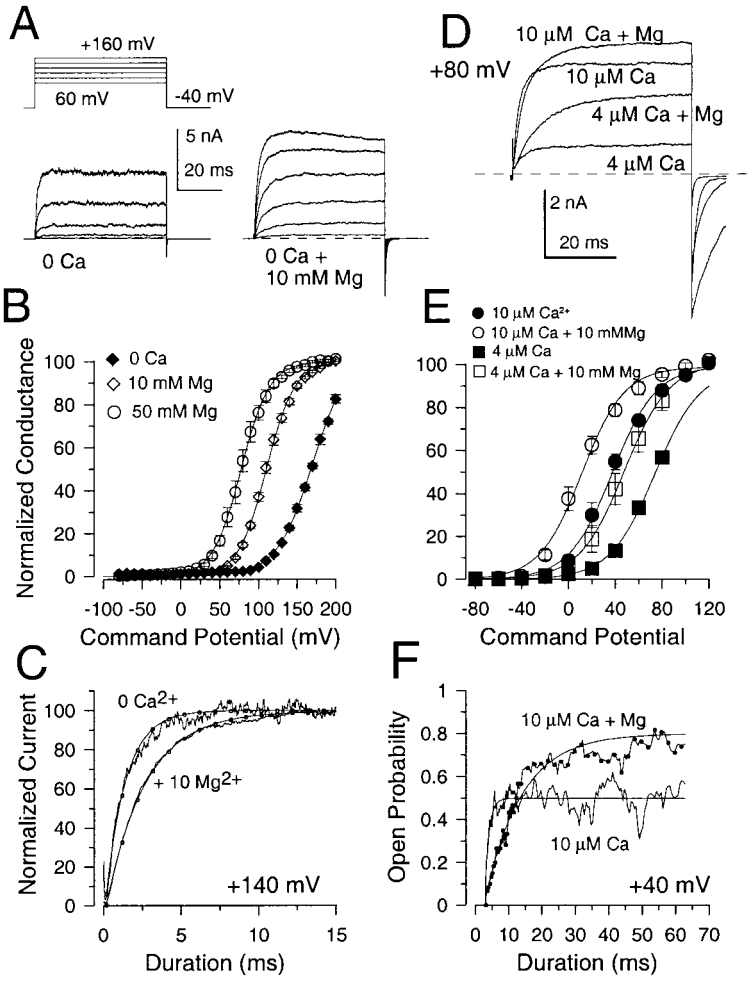

FIGURE 4. Mg^{2+} also shifts current activation in lower Ca^{2+} or 0 Ca^{2+}. In A, currents on the left were activated by the indicated protocol with a solution containing trace Ca^{2+} with 10 mM EGTA. On the right, currents were activated from the same patch with a solution containing 0 Ca^{2+}, 5 mM EGTA but with 10 mM Mg^{2+}. In 0 Ca^{2+}, time constants of activation (τ_a) were 1.85, 1.50, 1.12 ms for +120, +140, and +160 mV, respectively. With 10 mM Mg^{2+}, τ_a was 4.0, 2.72, and 2.22 ms at +120, +140, and +160 mV, respectively. In B, the normalized conductance is plotted as a function of command potential for 0 Ca^{2+} (eight patches), 10 mM Mg^{2+} (eight patches) and 50 mM Mg^{2+} (seven patches). Conductance values were normalized in each patch to the maximum value obtained with 50 mM Mg^{2+}. Fits of Eq. 1 (solid lines) yielded values for $V_{0.5}$ of 170.7 ± 2.6 mV (k = 23.6 mV) for 0 μM Ca^{2+}, 110.5 ± 0.6 mV (k = 18.3 mV) for 10 mM Mg^{2+}, and 78.0 ± 0.5 mV (k = 18.3 mV) for 50 mM Mg^{2+}. In C, currents activated at +140 mV were normalized to peak steady-state amplitude of a single exponential fit to the rising phase of currents activated either with 0 Ca^{2+} or with 0 Ca^{2+} + 10 mM Mg^{2+}. The time constant of activation with 0 Ca^{2+} was 1.50 ms, whereas with 10 mM Mg^{2+} was 2.72 ms. The slowing of activation with Mg^{2+} was consistently observed at all activation voltages and argues that the additional activation by Mg^{2+} is not the result of an increase in trace Ca^{2+}. In D, currents were activated by a voltage step to +80 mV with either 4 or 10 μM Ca^{2+} without or with the addition of 10 mM Mg^{2+}. Unbuffered divalent cation solutions were prepared as described in the MATERIALS AND METHODS. Note the increased current amplitude and slower activation of current in the presence of Mg^{2+}. In E, G-V curves were constructed from measurement of tail currents from a set of 4 patches studied as in D. Error bars represent the SEM of four patches. The $V_{0.5}$ for each curve is 37.6 ± 1.8 mV (10 μM Ca^{2+}), 11.6 ± 2.5 (10 μM Ca^{2+} + 10 mM Mg^{2+}), 73.8 ± 1.1 mV (4 μM Ca^{2+}), and 47.8 ± 1.1 mV (4 μM Ca^{2+} plus 10 mM Mg^{2+}). Buffered Ca^{2+} solutions prepared at the same time and tested on the same patches yielded $V_{0.5}$ values of 36.2 ± 1.6 mV for 10 μM Ca^{2+} and 71.2 ± 1.2 mV for 4 μM Ca^{2+}. In F, ensemble averaged currents were generated from channels activated with the indicated solutions for a voltage-step to +40 mV from a patch containing two channels. The addition of Mg^{2+} increases the open probability towards maximal values but slows down the time constant of current activation. With 10 μM Ca^{2+}, the activation time constant was 1.4 ± 0.3 ms, whereas with 10 μM Ca^{2+} plus 10 mM Mg^{2+} the time constant was 11.1 ± 0.5 ms.

mal to near maximal. If Mg^{2+} produced a shift in $V_{0.5}$ by simply shifting the effective activation voltage by ~30–50 mV, an increase in activation rate would have been expected. This is clearly not observed. This leaves us with the possibility that the slowing of activation time course reflects inhibition by Mg^{2+} of Ca^{2+} binding, when [Mg^{2+}] sufficiently exceeds [Ca^{2+}].

A Low Affinity, Relatively Nonselective Divalent Cation Binding Site May Account for the Effects of Mg^{2+} and Ca^{2+}

Fig. 5 A summarizes the ability of Mg^{2+} to shift $V_{0.5}$ for currents activated by 300 μM Ca^{2+} for two separate sets of patches. For both sets of patches, the shift in $V_{0.5}$ at 100 mM Mg^{2+} is less than at 50 mM Mg^{2+}. The reduction in shift with 100 mM Mg^{2+} is the result expected, if Mg^{2+} inhibits the ability of 300 μM Ca^{2+} to shift gating. Because of this possible inhibitory action of Mg^{2+}, it is more difficult to ascertain whether the shift in $V_{0.5}$ produced by Mg^{2+} exhibits saturation. However, because of the saturation in the shift of $V_{0.5}$ observed over the range of 20–100 mM Ca^{2+}, it seems likely that the effects of Mg^{2+} also exhibit a similar saturation. However, it should be noted that both in our experiments and the experiments of Shi and Chi (2001b) additions of Mg^{2+} over the range of 10–100 mM to 0-Ca^{2+} solutions do not result in full saturation of the shift in $V_{0.5}$.

Another interesting aspect of the action of Mg^{2+} is the magnitude of the shift in $V_{0.5}$ produced by 10 mM Mg^{2+} at various [Ca^{2+}] up through 10 mM (Fig. 5 B). The results in Fig. 5 B include data from a variety of experimental conditions (Solaro et al., 1995), including estimates of single-channel open probability from one and two channel patches and macroscopic current estimates. Over the range of ~30 μM–1 mM Ca^{2+}, 10 mM

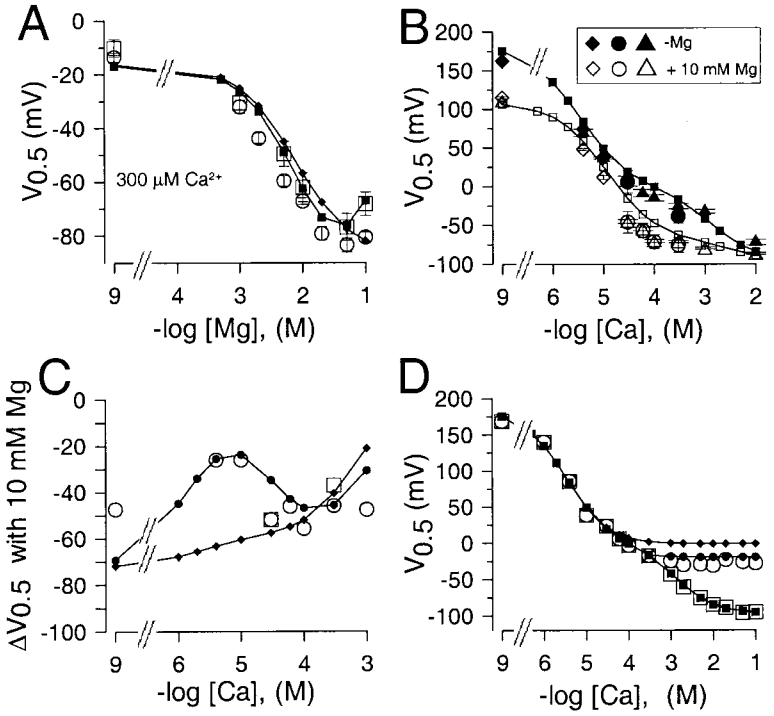

FIGURE 5. The ability of mM concentrations of Ca^{2+} and Mg^{2+} to shift G-V curves is similar. In A, the $V_{0.5}$ for activation is plotted as a function of Mg^{2+} for G-V curves obtained in two separate sets of patches each activated by 300 μM Ca^{2+} plus the indicated Mg^{2+}. The predictions for the shift in $V_{0.5}$ as a function of Mg^{2+} based on two sets of fitted values for Scheme I (Table II, columns A [◆] and D [■]) are also displayed. In B, the ability of Mg^{2+} to shift $V_{0.5}$ at different Ca^{2+} is displayed. Triangles show $V_{0.5}$ values from macroscopic currents without (▲) or with (△) 10 mM Mg^{2+}. Circles ([●] no Mg^{2+}; [○]: + 10 mM Mg^{2+}) are means and SD for $V_{0.5}$ determined from P_o measurements from four patches with either one or two channels as in Fig. 3. Diamonds ([◆] no Mg^{2+}; [◇] +10 mM Mg^{2+}) are values obtained with unbuffered Ca^{2+} solutions. Predictions from the fitted values for Scheme I (Table II, column D) are also shown for Ca^{2+} alone (■) and with 10 mM Mg^{2+} (□). In C, the change in $V_{0.5}$ ($\Delta V_{0.5}$) produced by 10 mM Mg^{2+} at different [Ca^{2+}] is displayed for macroscopic current measurements (○) and single-channel estimates (■). Estimates of predicted $\Delta V_{0.5}$ based on a fit of Scheme I to G-V curves with or without Mg^{2+} are also shown for two cases: first, Mg^{2+} inhibition of the high affinity site is allowed (●; Table II, column D) and no inhibition by Mg^{2+} occurs (◆; Table II; column F). In D, values of $V_{0.5}$ obtained as a function of Ca^{2+} (□) are replotted along with estimates of the $V_{0.5}$ corrected at Ca^{2+} of 1 mM and above by the additional shift produced by Mg^{2+} shown in A obtained with 300 μM Ca^{2+}. These values (○) provide an indication of the ability of the higher affinity, Ca^{2+} selective site to shift activation of BK channels, in the absence of the low affinity effect, assuming that the high and low affinity effects are independent and additive. Predicted values for $V_{0.5}$ based on a fit of Scheme I are also shown for the case of both low and high affinity Ca^{2+} binding sites (■; Table II; column D), and also for Ca^{2+} action alone in the absence of a high affinity site (◆). The latter values were also corrected for the approximately −17-mV shift that 300 μM Ca^{2+} should produce by acting at the low affinity sites (●). The discrepancy between the Mg^{2+} corrected data and the prediction from Scheme I arises from the fact that the Mg^{2+} correction was obtained with solutions with 300 μM Ca^{2+} such that the effect of 300 μM Ca^{2+} on the low affinity site is not taken into account.

Mg^{2+} seems to produce a rather constant shift of about −40 to −60 mV. Similarly, the shift at 0 Ca^{2+} is also about −50 mV. However, when 10 mM Mg^{2+} is added to 10-mM Ca^{2+} solutions, the resulting shift is substantially reduced. This latter effect is consistent with the idea that Mg^{2+} and Ca^{2+} are competing for a saturable, low affinity binding site. The magnitude of the shift caused by 10 mM Mg^{2+} over all Ca^{2+} is summarized in Fig. 5 C. Fig. 5 (B and C) also includes data obtained with unbuffered 4- and 10-μM Ca^{2+} solutions in which the shifts produced by 10 mM Mg^{2+} were only about −25 mV, similar to the results of Shi and Cui (2001b). In general, the ability of Mg^{2+} to shift gating over all [Ca^{2+}] qualitatively supports the idea that, even under conditions where the higher affinity site is only partially occupied by Ca^{2+}, Mg^{2+} still produced substantial shifts in gating and does so without substituting for Ca^{2+} at the higher affinity sites.

Because of the possibility that the effect described here may reflect an important regulatory role of free cytosolic Mg^{2+}, we also examined the ability of Mg^{2+} to shift activation, when Mg is added as MgATP. When Mg^{2+} is added as 2 mM Mg-ATP, solutions with nominal 100 μM Ca^{2+} are much less effective at activating current. ATP will bind both Mg^{2+} and Ca^{2+}. Based on published stability constants (Martell and Smith, 1974), the solution used here (100 μM added Ca^{2+}, 2 mM added MgATP) is calculated to have 33 μM free Ca^{2+} and 407 μM free Mg^{2+}. The $V_{0.5}$ observed for the solution containing 2 mM added MgATP (−6.3 ± 1.3 mV) is similar to that which would be expected for a 30-μM Ca^{2+} solution (about +8 mV) with an additional negative shift of ~10 mV resulting from 400 μM Mg^{2+}. Thus, the experiment is consistent with the idea that the shift produced by high Mg^{2+} depends on the free Mg^{2+} concentration, and that ATP reduces both free Ca^{2+} and free Mg^{2+}.

The shift caused by increasing [Mg^{2+}] from 1 to 10 mM is ~45–50 mV, whereas the shift caused by increases in [Ca^{2+}] from 1 to 10 mM is also ~50 mV. Thus, high concentrations of Ca^{2+} and Mg^{2+} may be acting at the same site(s) on the channel protein to modulate BK channel gating, independent of the action of Ca^{2+} at the higher affinity, Ca^{2+}-specific sites. This implies that there are at least two types of Ca^{2+} binding sites that are important for channel function. First, there are high affinity, relatively Ca^{2+}-specific sites

that, along with depolarization, produce channel opening. Second, there are low affinity sites that can bind either Ca^{2+} or Mg^{2+} to potentiate activation of channels, no matter whether channels are activated in the presence or absence of Ca^{2+}.

If we assume that high concentrations of Ca^{2+} and Mg^{2+} bind to the same or similar sites and are able to promote activation of *Slo1* currents in a similar fashion, then the results in Fig. 5 A can be used to "subtract" the effect of Ca^{2+} at the putative low affinity site from the $V_{0.5}$-pCa relationship shown in Fig. 2 E. This manipulation would then reveal the effect of Ca^{2+} acting only at the putative high affinity sites. This makes the assumption that the effects of high and low affinity sites on $V_{0.5}$ are independent, an issue which is addressed below. The consequences of this assumption are presented in Fig. 5 D. The open squares are $V_{0.5}$ values resulting from the action of $[Ca^{2+}]$ reproduced from Fig. 2 E. The additional shift in $V_{0.5}$ resulting from higher $[Ca^{2+}]$ were then assumed to be equivalent to the additional shift in $V_{0.5}$ resulting from high $[Mg^{2+}]$. Therefore, the closed squares were obtained by subtracting the magnitude of the shift of $V_{0.5}$ caused by a given $[Mg^{2+}]$ in the presence of 300 μM Ca^{2+} (Fig. 5 A) from the $V_{0.5}$ measured in the presence of the identical $[Ca^{2+}]$, but without Mg^{2+}. For example, the $V_{0.5}$ measured at 2 mM Ca^{2+} was shifted positive by the amount of shift caused by 2 mM Mg^{2+}. Thus, assuming Ca^{2+} and Mg^{2+} act equivalently at the same (or similar) binding site(s), the closed squares reflect the action of Ca^{2+} at the higher affinity sites alone. Once a correction is made for the effect of Ca^{2+} on low affinity binding sites, it is evident that for $[Ca^{2+}]$ greater than ~300 μM, the corrected $V_{0.5}$'s are no longer shifted negative by additional Ca^{2+}, even though activation remains voltage-dependent. This is consistent with the idea that high affinity, Ca^{2+}-dependent steps leading to activation are separate from voltage-dependent steps (Wei et al., 1994; Cox et al., 1997a; Horrigan and Aldrich, 1999; Horrigan et al., 1999). Another way of thinking about this is that the relationship between $V_{0.5}$ and Ca^{2+} in the presence of 10 mM Mg^{2+} is essentially constant from 100 μM to 100 mM (Fig. 5 B). Thus, the channel is essentially unaffected by changes in $[Ca^{2+}]$ over two orders of magnitude, although gating continues to be controlled by voltage.

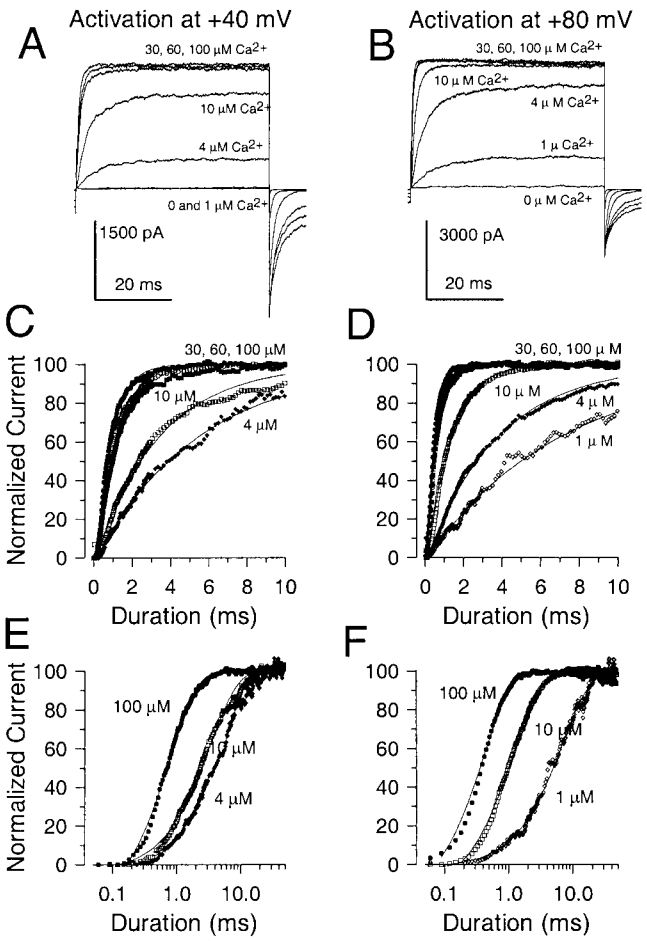

FIGURE 6. The current activation rate increases substantially as Ca^{2+} is raised from 1 μM to 100 μM. In A, currents were activated by a voltage step to +40 mV with Ca^{2+} concentrations of 0, 1, 4, 10, 30, 60, and 100 μM as indicated. In B, currents were activated in the same patch by a voltage-step to +80 mV with the same Ca^{2+} concentrations. In C, currents activated by the step to +40 mV were normalized to their maximal amplitude and fit with single exponentials. The activation time constants (τ_a) were 5.45, 3.38, 1.21, 1.05, and 0.80 ms, for 4, 10, 30, 60, and 100 μM, respectively. In D, the normalized current activation time course for the voltage-steps to +80 mV are shown. τ_a's were 7.08, 3.77, 1.23, 0.53, 0.46, and 0.39, for 1, 4, 10, 30, 60, and 100 μM Ca^{2+}, respectively. In E and F, the same normalized traces shown in C and D are plotted on a logarithmic time base to show the shift in activation time course with Ca^{2+}. An increase in Ca^{2+} from 1 to 10 μM produces a similar three to fourfold change in activation rate as the increase from 10 to 100 μM. At +40 mV, the trace in response to 4 μM Ca^{2+} is plotted since at 1 μM there is almost no detectable current activation.

Concentrations of Ca^{2+} and Mg^{2+} of 1 mM and above Have Minor Effects on Current Activation Rates at Potentials from +40 mV and More Positive

The above results argue that, at Ca^{2+} or Mg^{2+} concentrations of 1 mM and above, leftward shifts in the open probability of BK channels result primarily from the action of divalent cations at a relatively nonselective site distinct from higher affinity sites that specifically mediate Ca^{2+}-dependent gating of the channel. If $[Ca^{2+}]$ or $[Mg^{2+}]$ at ≥1 mM potentiates activation by acting at a site distinct from the Ca^{2+} binding site that regulates activation at lower $[Ca^{2+}]$, effects of higher $[Ca^{2+}]$ or $[Mg^{2+}]$ concentrations on channel gating kinetics might be distinct from those of more modest $[Ca^{2+}]$. The activation and deactivation behavior of *Slo1* currents at $[Ca^{2+}]$ up to ~1 mM has previously been examined in some detail (Cox et al., 1997a; Cui et

al., 1997). Here, we have examined the effects of $[Ca^{2+}]$ at up to 10 mM, and also examine current activation and deactivation in the presence of Mg^{2+}.

The rate of *Slo1* current activation was examined in inside-out patches as a function of both $[Ca^{2+}]$ and voltage with sampling rates and command steps of sufficient duration to allow determination of activation time course. Over a wide range of $[Ca^{2+}]$ and voltage, the activation time course was approximately exponential in nature (Fig. 6), although some initial delay in activation was observed. Representative currents activated at either +40 or +80 mV with $[Ca^{2+}]$ of 1–100 μM are shown in Fig. 6 (A and B). In Fig. 6, C and D, the currents were normalized to their maximal steady-state amplitude and each fit to a single exponential. To facilitate comparison of changes in activation rate, the normalized current activation time course for currents activated over approximately two orders of magnitude of $[Ca^{2+}]$ is plotted on a logarithmic time base in Fig. 6, E and F. At both +40 and +80 mV, 10-fold changes in concentration produce an approximately three to fivefold change in activation rate over this range of $[Ca^{2+}]$. In Fig. 7, A and B, currents activated by 300 μM, 1 mM, and 10 mM Ca^{2+} are plotted for both +40 and +80 mV. The normalized currents are plotted on both a linear scale (Fig. 7, C and D) and logarithmic time base (Fig. 7, E and F) showing that the increase in $[Ca^{2+}]$ from 300 μM to 10 mM results in only a small additional increase in activation rate, compared with the large changes seen in Fig. 6.

The effect of mM Mg^{2+} on τ_a was examined as above. The effects of 1 and 10 mM Mg^{2+} on currents activated with 300 μM Ca^{2+} are displayed in Fig. 8 (A and B). At 10 mM Mg^{2+}, there is a substantial shift in the G-V curve and substantial open channel block, but the activation course is similar to that in the absence of Mg^{2+}. Comparison of the activation time course of the normalized currents either on a linear (Fig. 8, C and D) or logarithmic (Fig. 8, E and F) time base further emphasizes the lack of effect of Mg^{2+} on τ_a in the presence of 300 μM Ca^{2+}. Thus, at potentials where additional depolarization would enhance current activation rate, concentrations of Ca^{2+} and Mg^{2+} above 1 mM have little effect on current activation rates. Thus, the lack of effect of Mg^{2+} on τ_a indicates that, whatever the mechanism of action of Mg^{2+} (and mM Ca^{2+}), it does not affect the voltage-dependent rate limiting activation steps.

The dependence of τ_a on voltage is plotted for 0–300 μM Ca^{2+} in Fig. 9 A and for 300 μM–100 mM Ca^{2+} in Fig. 9 B. Again at Ca^{2+} above 300 μM, the change in τ_a is much smaller than at lower $[Ca^{2+}]$. Furthermore, at each $[Ca^{2+}]$, the dependence of τ_a on voltage is similar. There appears to be an anomalous aspect of the effect of Ca^{2+} on activation in comparing the results at 0 and 1 μM Ca^{2+}. Specifically, there is a slowing of activation at potentials of +100 mV and more positive as $[Ca^{2+}]$ is elevated to 1 μM, whereas activation is again faster at 4 μM. We have not examined other concentrations over the range of 0 to 4 μM. This result is consistently observed in different sets of patches both in our own experiments and those of others (Cui, J., personal communication). For comparison to the effects of Ca^{2+}, the effect of 1 to 100 mM Mg^{2+} on current activation elicited with 300 μM Ca^{2+} is shown in Fig. 9 C. Over the range of −60 through +190 mV, Mg^{2+} is essentially without effect on current activation rates, with only some slowing of activation at 50 and 100 mM Mg^{2+}.

Time constants were converted to activation rates and the mean rate of activation is plotted as a function of $[Ca^{2+}]_i$ from 1 μM to 50 mM in Fig. 9 D for poten-

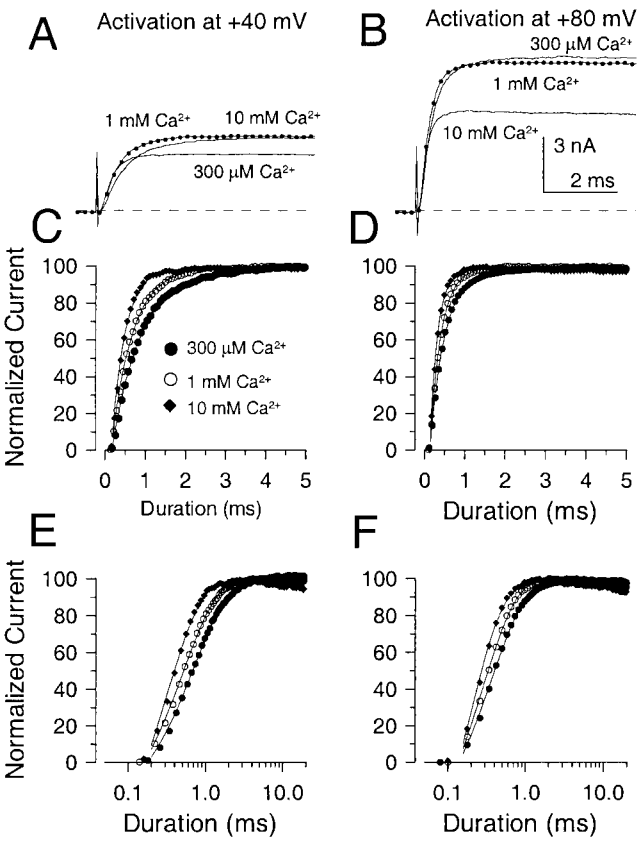

FIGURE 7. Increases of Ca^{2+} from 300 μM to 10 mM produce smaller increases in current activation time rate. In A and B, currents were activated by 300 μM, 1 mM, and 10 mM Ca^{2+} at either +40 mV (panel A) or +80 mV (panel B). In C and D, each trace in A and B was normalized to the maximal current amplitude to compare the activation time course. Points show every fourth digitized current value. Solid lines are the best fit of a single exponential function to the activation time course. At +40 mV, the activation time constant (τ_a) was 0.73, 0.52, and 0.33 ms for 300 μM, 1 mM, and 10 mM Ca^{2+}, respectively. At +80 mV, τ_a was 0.38, 0.28, and 0.19 ms for 300 μM, 1 mM, and 10 mM Ca^{2+}, respectively. In E and F, the normalized current activation time course is plotted on a logarithmic time base to allow better comparison of the relatively small concentration dependence of the activation rate for this 30-fold change in concentration compared with that shown in Fig. 6.

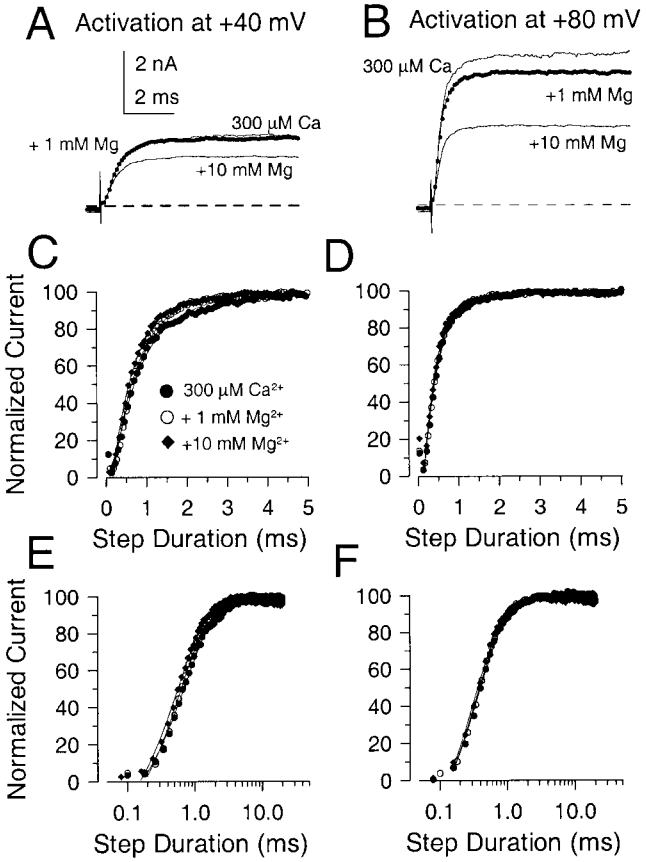

FIGURE 8. Addition of Mg^{2+} concentrations which markedly shift G-V curves does not increase the limiting rate of *Slo1* current activation. In A and B, traces were elicited in each panel with 300 μM Ca^{2+} alone, and with 300 μM Ca^{2+} with either 1 mM or 10 mM Mg^{2+}. Traces on the left were activated by a voltage step to +40 mV and, on the right, to +80 mV. In C and D, the normalized current activation time course is plotted on a linear time base (every fourth digitized value is plotted), while, in E and F, the same traces are shown on a logarithmic time base. Solid lines are fits of a single exponential function to the activation time course. At +40 mV, τ_a was 0.75, 0.64, and 0.59 ms for 300 μM Ca^{2+}, 300 μM Ca^{2+} + 1 mM Mg^{2+}, and 300 μM Ca^{2+} + 10 mM Mg^{2+}, respectively. At +80 mV, τ_a was 0.38, 0.36, and 0.33 ms for each solution. Raising Mg^{2+} up to 10 mM results in little effect on the time course of current activated in the presence of 300 μM Ca^{2+}.

tials of +20, +60, +100, and +140 mV. The rate of activation at a given voltage increases markedly with increases in $[Ca^{2+}]$ up to ~1 mM before exhibiting saturation over millimolar concentrations that still produce additional shifts in GV curves. The dependence of activation rate on $[Ca^{2+}]$ (ignoring the rate at 0 Ca^{2+}) was fit with the following function:

$$k(Ca) = k_{min} + \frac{k_{max} - k_{min}}{1 + ([Ca]/K_D)^n}, \quad (2)$$

where k(Ca) is the rate of activation at a given $[Ca^{2+}]$, k_{min} is the minimal activation rate, k_{max} is the limiting rate at saturating $[Ca^{2+}]$, K_D is the concentration of half-maximal Ca^{2+} effect, and n is a Hill coefficient. The limiting activation rate increases with depolarization at and above 1 μM $[Ca^{2+}]$, while the apparent K_d is also shifted to lower concentrations with depolarization. The Hill coefficient shows little variation with voltage.

The saturation in *Slo1* current activation rate is consistent with the idea that a key Ca^{2+}-dependent step no longer influences current activation rates at $[Ca^{2+}]$ above 1 mM. However, despite the fact that additional elevations in $[Ca^{2+}]$ do not increase the activation rate, additional depolarization can result in faster current activation. Thus, the saturation in the Ca^{2+} dependence of activation rate is unrelated to any limit on the channel activation process itself. Rather, the limiting activation rate at saturating $[Ca^{2+}]_i$ does vary with voltage, consistent with the idea that solely voltage-dependent transitions determine the limiting rate of activation at $[Ca^{2+}]$ of 1 mM and above.

The effect of Mg^{2+} on current activation is summarized in Fig. 9 E. When currents were activated with 300 μM Ca^{2+}, additions of $[Mg^{2+}]$ from 1 through 100 mM resulted in no additional increase in current activation rate. In fact, at $[Mg^{2+}]$ above 10 mM, a slowing in the activation rate was observed, consistent with the idea that Mg^{2+} may inhibit Ca^{2+} binding at the low affinity activation site (Shi and Cui, 2001b). We also examined the effect of Mg^{2+} on activation of current with 0 Ca^{2+}/5 mM EGTA. It was shown earlier that Mg^{2+} slows current activation with 10 μM Ca^{2+} (Fig. 5), an effect probably resulting from an inhibitory effect of Mg^{2+} on the high affinity Ca^{2+} binding site. However, with 0 Ca^{2+}, there was essentially no effect of 10 mM Mg^{2+} on activation time constant at potentials positive to +160 mV, whereas at more negative potentials and less than maximal open probabilities, activation and deactivation were slowed, both effects probably resulting from the effects of Mg^{2+} on transitions involved in deactivation described below. Thus, Mg^{2+} does not appear to directly influence rate limiting, voltage-dependent activation steps in the absence of Ca^{2+}. However, it should be noted that, with 0 Ca^{2+} and $[Mg^{2+}]$ above 10 mM, we also observed an increase in current activation rate (Fig. 9 E) that cannot be easily accounted for by the mechanisms presented below.

Deactivation Is Slowed by Either Increases in Ca^{2+} or Mg^{2+}

Deactivation tails resulting from closure of *Slo1* channels after repolarization were examined over a range of potentials with $[Ca^{2+}]$ from 0 μM to 100 mM. Deactivation, under most conditions, could be described by a single exponential. The deactivation time constant (τ_d) is plotted as a function of voltage in Fig. 10 A over Ca^{2+} concentrations spanning six orders of magnitude. Similarly, τ_d is plotted as a function of voltage in Fig. 10 B for solutions containing 300 μM Ca^{2+} with or without

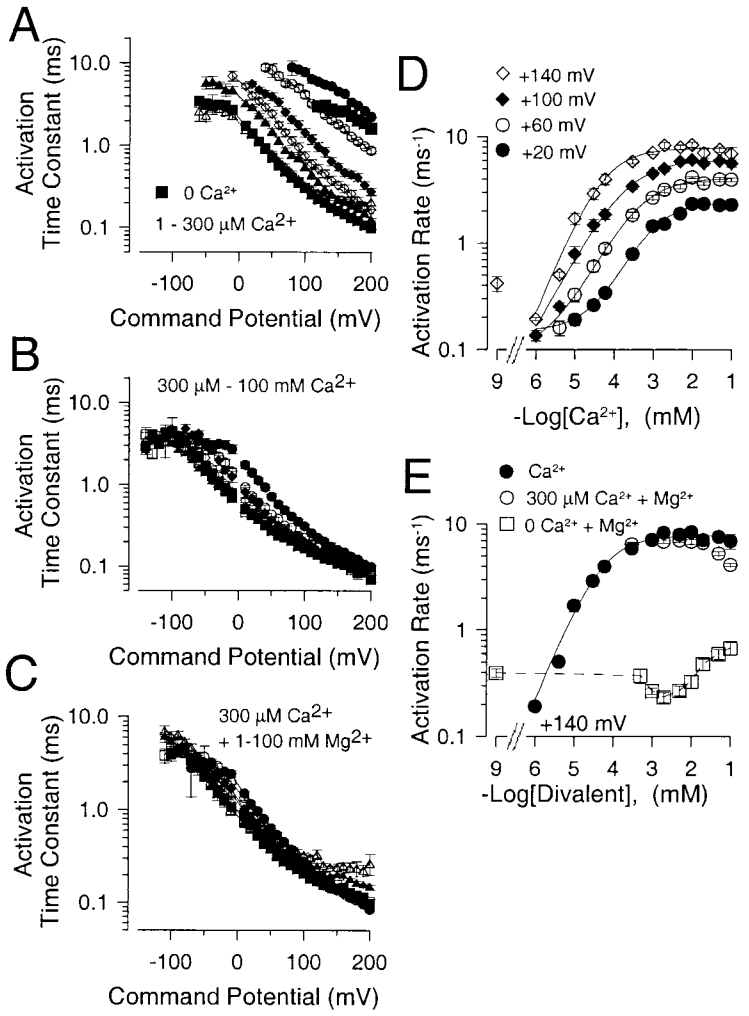

FIGURE 9. Millimolar concentrations of either Ca^{2+} or Mg^{2+} are similar in their effects on current activation rates. In A, the time constant of activation (τ_a) is plotted as a function of command potential for Ca^{2+} concentrations of 1 μM (●), 4 μM (○), 10 μM (◆), 30 μM (◇), 60 μM (▲), 100 μM (△), and 300 μM (■). Error bars in A and B are SEM for 4-13 patches. In B, τ_a is plotted as a function of command potential for Ca^{2+} concentrations of 300 μM (●), 1 mM (○), 2 mM (◆), 5 mM (◇), 10 mM (■), 20 mM (□), 50 mM (▲), and 100 mM (△). In C, τ_a is plotted as a function of command potential for solutions containing 300 μM with added Mg^{2+} of 0 mM (●), 1 mM (○), 2 mM (◆), 5 mM (◇), 10 mM (■), 20 mM (□), 50 mM (▲), and 100 mM (△). Each point shows the mean and SEM of 4-11 patches. In D, the mean rate of current activation for *Slo1* currents is plotted as a function of Ca^{2+} for command potentials of +20 (●), +60 (○), +100 (◆), and +140 (◇) mV. Error bars are SEM. Solid lines are fits of Eq. 2. At +20 mV, k_{max} was 2.4, K_d = 0.87 ± 0.30 μM, and n = 0.88 ± 0.28. At +60 mV, k_{max} was 4.1, K_d = 398 ± 160 μM, and n = 0.77 ± 0.20; at +100 mV, k_{max} = 6.0, K_d = 181 ± 59 μM, and n = 0.72 ± 0.14; at +140 mV, k_{max} = 7.7, K_d = 59 ± 25 μM, and n = 0.92 ± 0.32. Note the anomalous slowing of current activation rate at 1 μM Ca^{2+} relative to 0 μM at +140 mV. This point was not included in the fit. In E, current activation rate is plotted as a function of total divalent in the solution at +140 mV for solutions with no added Mg^{2+} (●) and solutions with Mg^{2+} added to 300 μM Ca^{2+} (○), showing that Mg^{2+} has little effect on the limiting rate of current activation, although additional depolarization will produce an increase in current activation rate. Note the inhibition of activation rate at the highest [Mg^{2+}]. Current activation with 0 Ca^{2+} and various [Mg^{2+}] is also plotted (□), showing the relative lack of effect of Mg^{2+} in comparison to Ca^{2+}.

either 1, 10, or 100 mM Mg^{2+}. The dependence of τ_d on Ca^{2+} and Mg^{2+} appears similar but differs from the dependence of τ_a on Ca^{2+} and Mg^{2+}. Namely, increases in [Ca^{2+}] above 100 μM continue to result in additional slowing of current deactivation, implying that there may be Ca^{2+}-dependent effects at higher [Ca^{2+}] that influence rates of exit from open states or closed states near open states, but which have no affect on the limiting rates of channel activation. Similarly, although Mg^{2+} is without effect in substituting for Ca^{2+}-dependent activation steps, Mg^{2+} does slow deactivation in a fashion qualitatively similar to the effect of mM Ca^{2+}. For both Mg^{2+} and Ca^{2+}, the slowing of deactivation is substantial over the range of 1–10 mM of either cation, concentrations at which activation rates are unaffected. However, above 10 mM of either cation, there is an indication that the effect on deactivation exhibits saturation, which is consistent with the saturation in the shift of G-V curves at high divalent cation concentrations. The change in τ_d as a function of [Mg^{2+}] is plotted in Fig. 10 C and compared with the effect of a similar total concentration of divalent with Ca^{2+} alone. Millimolar concentrations of Mg^{2+} and Ca^{2+} appear similar in their effects on deactivation.

To summarize the similarities and differences in the effects of Ca^{2+} and Mg^{2+} on kinetic aspects of *Slo1* currents, effects of various [Ca^{2+}] and [Mg^{2+}] were compared in the same sets of patches. At any given [Ca^{2+}] and [Mg^{2+}], the relaxation time constant (deactivation and activation) exhibits an approximately bell-shaped dependence on voltage. In Fig. 11 A, 10 μM Ca^{2+} is shown to shift both activation and deactivation times constants to a somewhat similar extent compared with 0 Ca^{2+}, whereas with 300 μM Ca^{2+}, the effects on τ_d begin to diminish while effects on activation remain pronounced. In Fig. 11 B, 4 μM Ca^{2+} produces a leftward shift qualitatively similar to that with 10 μM, although smaller. 1 μM Ca^{2+} results in the unusual slowing of activation described above, producing a slowing of the principle time constant at all voltages. In Fig. 11, C and D, 10 and 50 mM Ca^{2+} are compared with 10 and 50 mM Mg^{2+}. 10 and 50 mM Ca^{2+} produce a similar leftward shift in the relaxation time constant. In contrast, with 10 mM Mg^{2+}, there is no apparent effect on current activa-

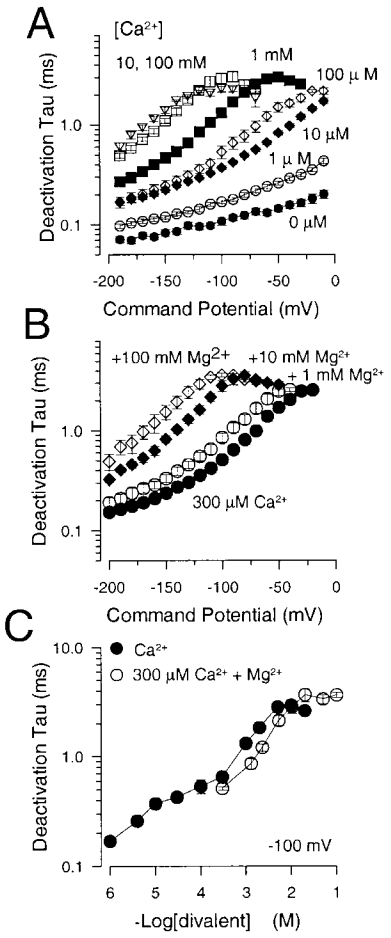

FIGURE 10. Millimolar concentrations of Mg^{2+} and Ca^{2+} have similar effects on current deactivation. In A, the deactivation time constants are plotted as a function of command potential for $[Ca^{2+}]$ spanning over six orders of magnitude, 1 μM–100 mM. Points and error bars are means and SEM of 5–15 patches. In B, the deactivation time constants are plotted as a function of command potential for tail currents obtained with 300 μM Ca^{2+} and 300 μM Ca^{2+} plus 1, 10, and 100 mM added Mg^{2+}. Points show means and SEM for 4–8 patches. In C, the deactivation time constant measured at −100 mV is plotted as a function of total [divalent] for solutions with only Ca^{2+} (●) and for solutions with 300 μM Ca^{2+} with added Mg^{2+} (○). The slowing of deactivation with either elevated Ca^{2+} or Mg^{2+} exhibits saturation, although at somewhat different concentrations.

tion, but deactivation is slowed. 50 mM Mg^{2+} produces some slight additional slowing in deactivation, but also results in some increase in current activation rate. In Fig. 11 E, 10 and 50 mM Ca^{2+} are shown to produce a substantial additional slowing of deactivation relative to 300 μM Ca^{2+}, with only weaker effects on current activation at positive potentials. The effects of 10 and 50 mM Mg^{2+} when added to 300 μM Ca^{2+} are quite similar (Fig. 11 F), producing a substantial slowing of current deactivation, with little effect on current activation, except for a clear slowing of activation at 50 mM. Thus, these kinetic effects remain generally consistent with the effects of Ca^{2+} and Mg^{2+} on GV curves. There is a higher affinity effect of Ca^{2+} that influences both current activation rates and deactivation rates. There is little evidence that Mg^{2+} acts at this site except for a slowing of activation, when $[Mg^{2+}]$ is perhaps at least three orders of magnitude greater than $[Ca^{2+}]$. In contrast, both Mg^{2+} and Ca^{2+} share an ability to slow deactivation at mM concentrations, while having minimal effects on limiting rates of current activation at these concentrations.

Mg^{2+} Increases the Hill Coefficient for Activation of Slo1 Current by Ca^{2+} by Shifting the Relationship between Hill Coefficient and Membrane Potential

One interesting aspect of the effect of Mg^{2+} reported in earlier studies was that Mg^{2+} increases the Hill coefficient for activation by Ca^{2+} of BK channels in bilayers (Golowasch et al., 1986) and that other divalent cations act similarly (Oberhauser et al., 1988). For gating by Ca^{2+}, the Hill coefficient is generally used as an indicator of the minimal number of Ca^{2+} ions that are required for channel activation. Where this has been examined for *Slo1* current, the Hill coefficient is typically around two with some tendency to increase with depolarization (Cui et al., 1997; Bian et al., 2001). Here, we addressed this issue in two ways. First, we examined the behavior of the Hill coefficient over a wider range of $[Ca^{2+}]$ than previously studied to assess how the proposed two binding sites might impact on Hill plots. Second, we determined whether effects of Mg^{2+} on the Hill coefficient would be reproduced here. To address the first issue, normalized conductance values from Fig. 2 C were replotted to display the relationship between conductance and $[Ca^{2+}]$ over a range of voltages (Fig. 12 A). Curves obtained at each command potential were fit with a Hill equation $G/G_{max} = B + A/[1 + (K_d/[Ca])^n$, where n is the Hill coefficient and K_d is the apparent Ca^{2+} dissociation constant. B is a term included to account for the Ca^{2+}-independent activation of current at the most positive activation potentials. At some voltages, this function did not describe the shape of the relationship between conductance and $[Ca^{2+}]$ very well. However, terms for the K_d (Fig. 12 C) and Hill coefficient (Fig. 12 D) were determined for voltages from −120 to +140 mV. The apparent affinity increases markedly with depolarization while appearing to reach a limiting value at the most negative activation potentials. The apparent Hill coefficient exhibits a surprisingly erratic appearance. However, consistent with other results (Cui et al., 1997), the Hill coefficient increases from ~1 to ~2.5 over the range of −20 to +80 mV. The error bars indicate the 90% confidence limits on the fitted parameter and indicate that the fitting function in some cases did not describe the shape of the curves very adequately. This sort of experiment suggests that two other factors are also likely to impact on estimates of Hill coefficient in various studies. First, large

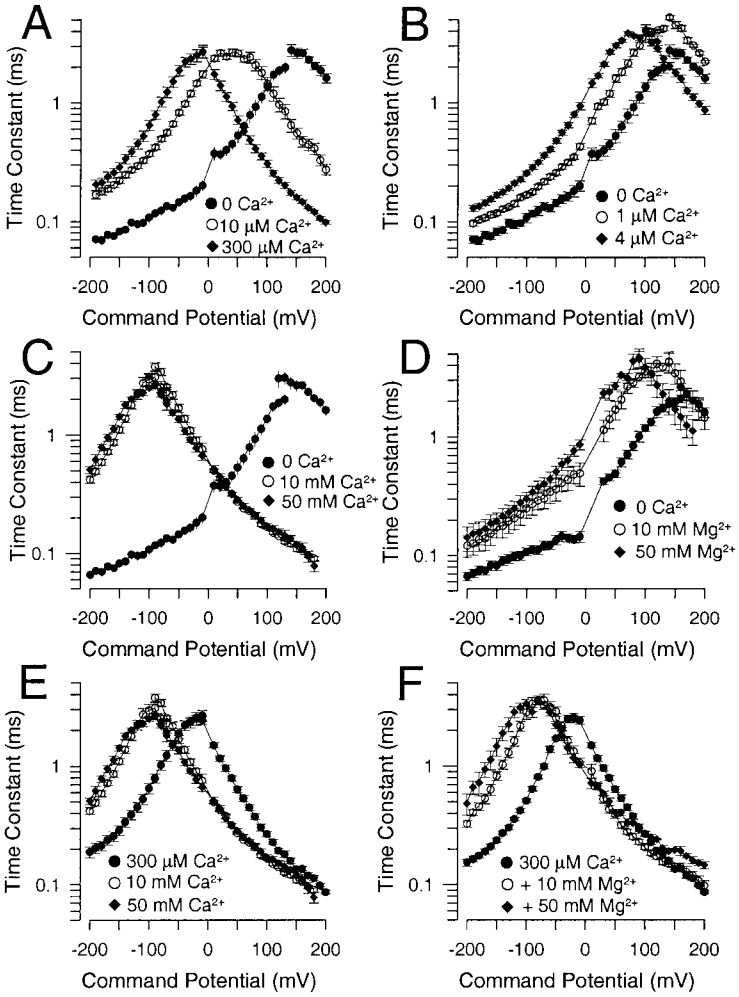

FIGURE 11. Comparison of effects of Ca^{2+} and Mg^{2+} on primary time constant of *Slo1* current relaxations. In A, activation and deactivation time constants obtained at 0, 10, and 300 μM Ca^{2+} are plotted as a function of potential. In B, the shift in relaxation time constant with 1 and 4 μM are compared with 0 μM Ca^{2+}. Note the unusual slowing of activation with 1 μM Ca^{2+}. In C, the effects of 10 and 50 mM Ca^{2+} are compared with 0 Ca^{2+}, whereas, in D, the effects of 10 and 50 mM Mg^{2+} are compared with 0 Ca^{2+}. In E, the effects of 10 and 50 mM Ca^{2+} are compared with 300 μM Ca^{2+}, whereas, in F, the effects of 10 and 50 mM Mg^{2+} plus 300 μM Ca^{2+} are compared with 300 μM Ca^{2+}.

variation in estimates of Hill coefficient might be expected to result from the fact that, in some studies, the number of Ca^{2+} concentrations over which the change in conductance is determined can be rather minimal. Second, at positive potentials where activation of current occurs in the absence of Ca^{2+}, if this activation is not taken into account, Hill coefficients will be estimated incorrectly. In sum, these results suggest that a typical Hill function may not be a mechanistically meaningful way of evaluating the Ca^{2+} dependence of *Slo1* current activation and that the apparent Hill coefficient may exhibit some unusual dependence on voltage. Possible reasons for this behavior are addressed below.

We next examined the effects of [Mg^{2+}] on the behavior of Hill plots. This analysis used a different set of patches than those used in Fig. 2 and used a more limited set of Ca^{2+} concentrations, but typical of those used in other investigations. Hill plots obtained for this data set in the absence of Mg^{2+} are shown for several voltages in Fig. 13 A, whereas similar plots in the presence of 10 mM Mg^{2+} are shown in Fig. 13 B. As above, the Hill equation was used to make estimates of K_d and the Hill coefficient. Given the more limited number of Ca^{2+} concentrations used in this set of patches, the estimate of Hill coefficient in particular exhibited large confidence limits. Both with and without Mg^{2+}, the K_d varied exponentially with command potential with a zero-voltage K_d of ~25 μM in the absence of Mg^{2+} and ~10 μM in the presence of Ca^{2+} (Fig. 13 C). Both with and without Mg^{2+}, there was a trend for the Hill coefficient to became larger at more positive potentials (Fig. 13 D), which is consistent with the observations in Fig. 12 D and other work (Cui et al., 1997). This increase in the Hill coefficient is, in part, the simple expectation of the fact that, for each increment in Ca^{2+}, G-V curves are shifted more at lower than at higher [Ca^{2+}], such that over the range of 100 μM–1 mM Ca^{2+}, little additional shift is observed (Wei et al., 1994; Cox et al., 1997b). As a consequence, at more negative potentials, relatively large increments in [Ca^{2+}] produce relatively small increases in conductance, resulting in a less steep Ca^{2+} dependence of activation. Since, as shown above, 10 mM Mg^{2+} produces an essentially 50-mV leftward shift of the G-V curve obtained at each [Ca^{2+}], this

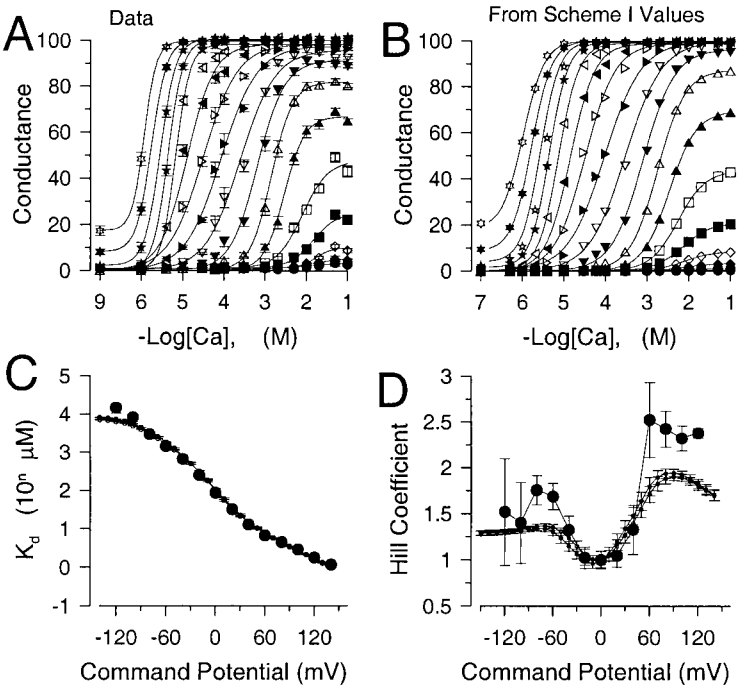

FIGURE 12. The behavior of K_d and Hill coefficient over all $[Ca^{2+}]$. In A, conductances given in Fig. 2 D were replotted to show the Ca^{2+} dependence of conductance at a given voltage. Each point is the mean and SEM for the estimate. Solid lines are fits of the modified Hill equation given in the text. Symbols correspond to potentials of −200 (●), −180 (○), −160 (◆), −140 (◇), −120 (■), −100 (□), −80 (▲), −60 (△), −40 (▼), −20 (▽), 0 (▶), +20 (▷), +40 (◀), +60 (◁), +80 (★), +100 (☆), +120 (closed six-pointed star), and +140 (open six-pointed star) mV. In B, conductance values predicted from Scheme I (see Fig. 14) based on values given in Table II (column D) were plotted as a function of $[Ca^{2+}]$ and fit with the modified Hill equation (solid lines). Symbols are as in A. In C, estimated values for the K_d for apparent Ca^{2+} affinity (●) obtained from fitting the data in Fig. 12 A are plotted as a function of command potential. The solid line with small filled circles corresponds to values for K_d predicted from Scheme I as shown in Fig. 12B. The line with small open circles corresponds to K_d values assuming no Mg^{2+} inhibition of the high affinity site. In D, the Hill coefficients determined from Fig. 12 A (●) are plotted as a function of voltage. Error bars represent the 90% confidence limit on the estimate of the Hill coefficient. The dotted lines show the predictions from Scheme I as determined from values in Table II, column D (Fig. 12 B, small closed circles) or from Table II, column F (small open circles, no Mg^{2+} inhibition).

would be expected to cause an apparent increase in Hill coefficient at any command potential. Another way of viewing the results is that the relationship between Hill coefficient and command potential (Fig. 13 D) is simply shifted leftward ~50 mV in the presence of Mg^{2+}. Thus, the present results suggest that Mg^{2+} does cause an increase in the apparent Hill coefficient for Ca^{2+} at a given voltage, but that this effect reflects a shift of the relationship between Hill coefficient and voltage along the voltage axis.

Mg^{2+} Produces Shifts of G-V Curves Resulting from α + β1 Subunit Coexpression

The ability of Mg^{2+} to shift G-V curves at a given Ca^{2+} is somewhat reminiscent of the effect of the β1 and β2 auxiliary subunits of BK channels (McManus et al., 1995; Meera et al., 1996; Wallner et al., 1999; Xia et al., 1999). If Mg^{2+} were acting to mimic the effects of an associated β subunit, Mg^{2+} might be ineffective on channels resulting from α + β subunit coexpression. To test this possibility, the effects of different concentrations of Mg^{2+} on α + β1 currents elicited with 100 μM Ca^{2+} were examined. Normalized G-V curves were generated for a set of four patches. The $V_{0.5}$ for current activation with 100 μM Ca^{2+} was −110.9 ± 1.5 mV, whereas, for 1, 2, 10, and 20 mM Mg^{2+}, values for $V_{0.5}$ were −123 ± 2.4 mV, −129.7 ± 1.6 mV, −140.0 ± 1.3, and −148.9 ± 1.3 mV, respectively. In this set of patches, the net effect of 10 mM Mg^{2+} is to shift the $V_{0.5}$ about −30 mV, which is less than observed in the absence of the β1 subunit. However, it is clear that Mg^{2+} is able to exert much of its effect, irrespective of the presence or absence of the β1 subunit.

Effects of Mg^{2+} Do Not Result from Changes in Ca^{2+} Binding Affinity

The primary effects of Mg^{2+} that require explanation are as follows. First, 10 mM Mg^{2+} appears to produce a similar shift in $V_{0.5}$ at both 0 and 300 μM Ca^{2+} with somewhat smaller shifts at 4 and 10 μM. Second, Mg^{2+} does not substitute for Ca^{2+} in the high affinity Ca^{2+}-dependent steps that participate in increases in current activation rate. Third, mM Mg^{2+} shares with mM Ca^{2+} the ability to slow deactivation, an effect which does not exhibit saturation until over 10 mM divalent. Finally, Mg^{2+} produces a slowing of current activation with 4 and 10 μM Ca^{2+} under conditions of near maximal current activation. Can these effects be accounted for by a single mechanism of action?

To guide our thinking, we first consider the particular 50-state model presented by Cox and Aldrich (2000) to account for the dependence of steady-state conductance on voltage and Ca^{2+}. The steady-state predictions of their formulation are summarized in the following equation:

$$P(V,Ca) = \frac{1}{1 + B\left[\frac{(1 + e^{ZF(V - Vh_c)/RT})}{(1 + e^{ZF(V - Vh_o)/RT})}\right]^4 L(0) e^{\frac{-QFV}{RT}}}, \quad (3)$$

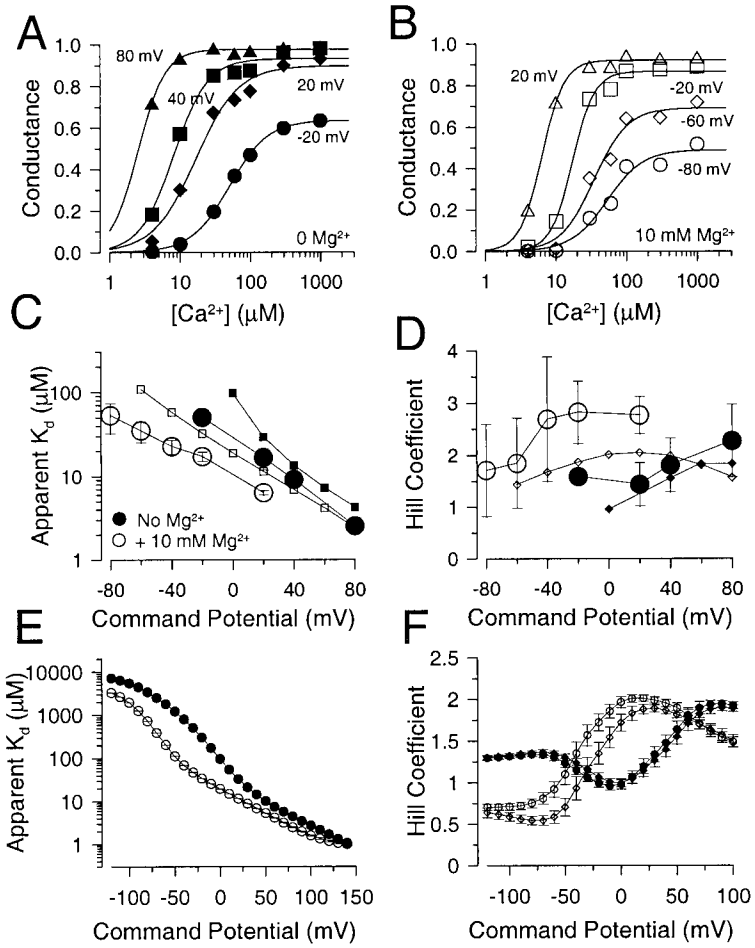

FIGURE 13. The apparent Hill coefficient for activation of conductance by Ca^{2+} is increased by Mg^{2+}. In A, each point is the estimate of conductance activated at a given Ca^{2+} and voltage obtained from normalized G-V curves. Solid lines are fits of the modified Hill equation given in the text. Fitted values for apparent K_d and Hill coefficient are plotted in C and D, respectively. Values used in this figure were from a different set of patches than shown in Fig. 2 or Fig. 12. In B, conductance estimates obtained in the presence of 10 mM Mg^{2+} are plotted as a function of Ca^{2+} for a range of voltages. At comparable voltages, the Hill coefficient for activation is higher in the presence of Mg^{2+}. In C, the apparent K_d (in μM) for activation of conductance by Ca^{2+} either in the absence (●) or presence (○) of 10 mM Mg^{2+} is plotted as a function of activation potential. The apparent Ca^{2+} affinity is increased at a given potential in the presence of Mg^{2+}. The error bars are 90% confidence limits from the estimates of $K_{0.5}$ obtained in A and B. Predictions from Scheme I (Table II, column D) for solutions without Mg^{2+} (■) or with Mg^{2+} (□) are also shown. In D, the Hill coefficient and confidence limits for the activation of conductance by Ca^{2+} either in the absence (●) or presence (○) of Mg^{2+} are plotted as a function of command potential, along with estimates (no Mg^{2+} [◆], +10 mM Mg^{2+} [◇]) from Scheme I based on estimates of Mg^{2+} affinities from column B of Table II. Both for experimental data and the theoretical predictions, there is a trend for increased Hill coefficient at more positive potentials and, at any given potential, Mg^{2+} increases the apparent Hill coefficient. In E, the K_d for Ca^{2+} effect predicted from Scheme I is plotted over a wider range of potentials. Both with (○) and without (●) 10 mM Mg^{2+}, at the most negative potentials a limit in the K_d is observed, while affinity increases dramatically with depolarization. In F, the behavior of Hill coefficient as a function of command potential predicted by Scheme I is displayed over a wider range of potentials. Predictions from scheme I assuming Mg^{2+} inhibition of the high affinity site (Table II, column D) are shown both without (●) and with (○) 10 mM Mg^{2+}. Predictions from scheme I with no Mg^{2+} inhibition (Table II, column F) are also shown without (◆) and with (◇) 10 mM Mg^{2+}.

where $B = [(1 + Ca/K_c)/(1 + Ca/K_o)]^4$ with K_c is the Ca^{2+} binding equilibrium for the closed channel, K_o is the Ca^{2+} binding equilibrium for the open channel, L(0) is the open-to-closed equilibrium constant when no voltage sensors are active and no Ca^{2+} binding sites are occupied, Q, the gating charge associated with this closed to open equilibrium, Vh_c, is the voltage at which a single voltage sensor is active half the time when the channel is closed, and Vh_o, is the voltage at which a single voltage sensor is active half the time when the channel is open, and Z is the equivalent gating charge associated with each voltage-sensor's movement. This formulation assumes that voltage-dependent transitions and Ca^{2+} binding transitions in each subunit are independent and that Ca^{2+} binding affinity is not influenced by movement of voltage sensors.

Might alteration by Mg^{2+} of any parameters in the above equation provide suggestions concerning how Mg^{2+} may produce relatively similar shifts in G-V curves at both 0 and 300 μM Ca^{2+}? To test this possibility, we empirically adjusted various parameters in Eq. 3 to ascertain whether any would reproduce the key features of the G-V curves, i.e., the relatively constant shift at all $[Ca^{2+}]$ and the increase in slope at 0 Ca^{2+}. Of all the possible parameters, only adjustment of two parameters were qualitatively able to mimic the effects of Mg^{2+}. First, adjustment of Vh_o, the term for the voltage at which a single voltage sensor is half the time active when the channel is open, could produce a relatively similar shift at all Ca^{2+} and increase the slope at 0 Ca^{2+}. Similarly, the magnitude of L(0) shifts the family of G-Vs in a somewhat parallel fashion along the voltage axis as shown previously (Cox and Aldrich, 2000). Thus, in accordance with the assumptions of this model, this would argue that the effects of Mg^{2+} might result from an increase in the stability of the open states perhaps either by stabilizing the voltage sensors in the active configuration or by simply affecting the equilibrium between the closed and open conformations. In contrast, the effects of Mg^{2+} are entirely inconsistent with any model in which Mg^{2+} might somehow change the affinity of Ca^{2+}, i.e., K_c or K_o.

A 250-state Allosteric Model Describes the Effects of Mg^{2+}

We next considered whether a particular stochastic model incorporating binding of Mg^{2+} might allow an explicit analytical evaluation of the effects of Mg^{2+}. We begin with the specific 50-state model proposed by Cox and Aldrich described above in which Ca^{2+} binding and voltage-sensor movement are not coupled. Based on the tetrameric nature of the channel (Shen et al., 1994), we postulate a Mg^{2+} binding site on each subunit. The result of the addition of four independent Mg^{2+} binding steps to the basic 50-state model is shown for one case in Scheme I. Basically, for each of the two tiers characteristic of the 50-state model, there are now four additional sets of the two tiers corresponding to binding of one, two, three, or four Mg^{2+} cations. Each pair of tiers corresponding to a different extent of ligation by Mg^{2+} is designated by I-V. Any state in I is connected to the corresponding state in II by a Mg^{2+} binding step. Similarly, any state in II is connected to the corresponding states in either I or III by Mg^{2+} dissociation and association, respectively. This is indicated in Scheme I by the pathways connecting the lower and leftmost state in each tier to the lower and leftmost states in adjacent tiers with constants determined by $K(l)_o$ and $K(l)_c$, the binding constants of a divalent cation to the low affinity site on either open or closed channels, respectively. This results in a total of 250 states, which results naturally from the fact that gating is regulated by three parameters, voltage, Ca^{2+}, and Mg^{2+} (or other divalent).

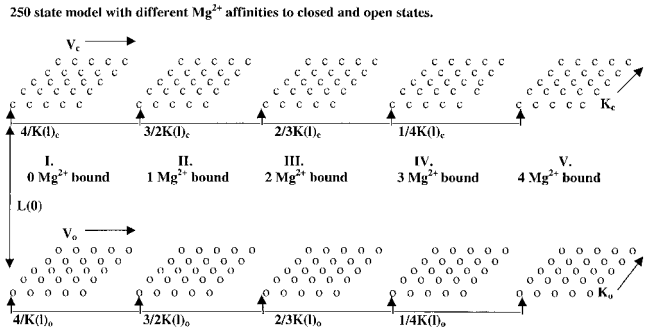

(SCHEME I)

Analytic evaluation of a 250-state model depends on specific assumptions about the relationship between Mg^{2+} binding steps and other transitions. Because the effects of Mg^{2+} are apparent in 0 Ca^{2+}, we exclude from consideration the case where binding of Mg^{2+} is assumed to influence either K_o or K_c, the affinities of Ca^{2+} to open or closed channels, respectively. Here, we first consider the case (given in Scheme I) in which we propose that binding of Mg^{2+} (or mM Ca^{2+}) to open and closed channels may occur with different affinities. This low affinity binding would have no effect on voltage-sensor equilibria or Ca^{2+} binding affinities. The shift in $V_{0.5}$ would be driven by the higher affinity with which Mg^{2+} binds to open states. This would be analogous to the binding of Ca^{2+} to its high affinity site, although independent of that effect. In essence, binding of Mg^{2+} would be coupled to changes in L(0) between adjacent pairs of tiers given in Scheme I.

For solution of steady-state equations for the 250-state model for Scheme I, in addition to the seven parameters required to describe the 50-state model in Eq. 3, the system is also defined by two additional parameters, $K(l)_o$ and $K(l)_c$, the affinity of Mg^{2+} (and or Ca^{2+}) to the low affinity divalent cation binding site when the channel is either open or closed, respectively. Fractional conductance for Scheme I as a function of [Ca^{2+}], voltage, and divalent cation concentration ([D]) is given by:

$$G(V,Ca,D) = \frac{1}{1 + B\left[\frac{1 + [D]/K(l)_c}{1 + [D]/K(l)_o}\right]^4 \left[\frac{(1 + e^{ZF(V - Vh_c)/RT})}{(1 + e^{ZF(V - Vh_o)/RT})}\right]^4 L(0) e^{\frac{QFV}{RT}}}, \quad (4)$$

where

$$B = \left[\frac{1 + [Ca]/K_c}{1 + [Ca]/K_o}\right]^4,$$

[D] corresponds to the concentration of divalent cation acting at the low affinity sites, and other parameters are as defined above. Despite the marked increase in number of states compared with the 50-state model, the form of the equation is similar to Eq. 3 with only two additional free parameters. For cases in which there are two species of divalent cations that may act at the low affinity sites, but with somewhat differing affinities, this expression is obviously not sufficient.

To examine the effects of Mg^{2+} and high Ca^{2+} in terms of Scheme I, we used four different data sets, each a set of patches obtained under a particular range of divalent cation concentrations. Set 1 entailed [Ca^{2+}] from 0 to 100 mM, set 2 used 0 Ca^{2+} with [Mg^{2+}] from 0 to 100 mM, set 3 used 300 μM Ca^{2+} with [Mg^{2+}] from 0 to 100 mM, and set 4 used both 0 and 300 μM with [Mg^{2+}] from 0 to 100 mM. In Fig. 14 A, it can be seen that the G-V curves from data set 1 can be quite well-described by Eq. 4. The displayed fit in Fig. 14 A is based on the values in Table I (column A). When L(0) was left unconstrained, the value converged within the range of 500,000–700,000 with very large confidence limits. Varying this value did not result in any improvement in the fit, which indicates that L(0) cannot be well-defined by this procedure. Of the parameters in Eq. 4, those pertaining to the Ca^{2+} binding steps are the most well constrained, whereas the parameters relating to movement

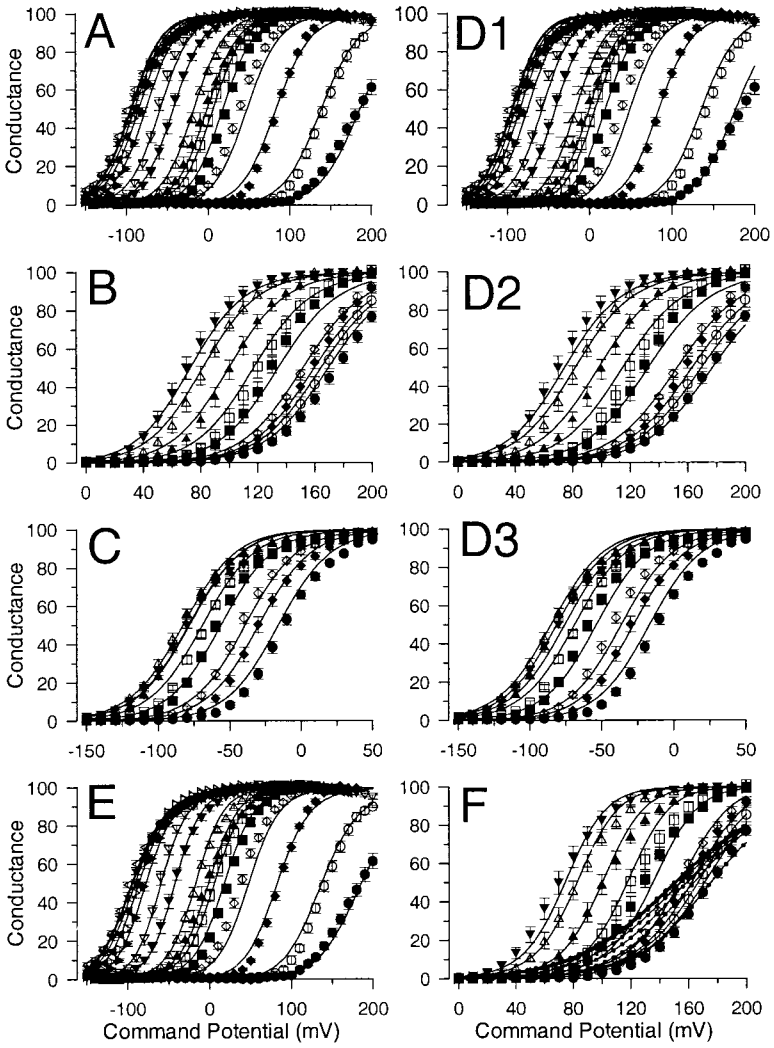

FIGURE 14. The dependence of *Slo1* conductance on Ca^{2+}, Mg^{2+} and voltage can be described by a 250 state allosteric model involving the independent action of Ca^{2+}, Mg^{2+} and voltage-sensor movement. In A, G-V curves obtained at different [Ca^{2+}] given in Fig. 2 D (data set 1) were fit with Eq. 4 with the solid lines resulting from the values given in column A, Table I. L(0) was constrained to 500000. In B, G-V curves obtained with 0 Ca^{2+} (●) plus 0.5 (○), 1 (◆), 2 (◇), 5 (■), 10 (□), 20 (▲), 50 (△), and 100 (5) mM Mg^{2+} (data set 2) were also fit with eq. 4, with parameters given in Table I, column B. In C, G-V curves obtained with 300 μM Ca^{2+} with [Mg^{2+}] from 0 to 100 mM (data set 3; symbols are as in B, but with no 0.5-μM points) were fit with eq. 5. The solid lines correspond to the fit resulting from the values given in column C, table I. Comparison of the values in columns A, B, and C indicate that quite similar values yield a good general description of G-V curves over all [Ca^{2+}], all [Mg^{2+}], and all voltages, except that the multiple Mg^{2+} binding affinities defined by Eq. 5 are not well-described in the fit to data set 3. In D1–D3, G-V curves shown in A-C were simultaneously fit with Eq. 5, yielding the values given in Table II (column D). Again, the general features of the shift in curves as a function of Ca^{2+} and Mg^{2+} is reasonably well-described. In E, G-V curves obtained over all [Ca^{2+}] were fit with Eq. 8, which assumes that Mg^{2+} influences the voltage-sensor equilibrium. Fitted curves correspond to values given in Table III (column A). In F, G-V curves at 0 Ca^{2+} were also fit with Eq. 8. When values obtained from fitting G-V curves at higher Ca^{2+} were used, it was not possible to obtain estimates for K_m and E that resulted in adequate descriptions of the data. The curves with open circles were generated from values in column C, Table III. L(0) was set to a value in which currents in 0 Ca^{2+} were well-described. However, the G-V curves at 10 and 50 mM Mg^{2+} could not be captured. However, when more parameters were left unconstrained, Eq. 8 could yield a fit that captured the G-V curves in 0 Ca^{2+} (smaller closed circles), but these values (column D, Table III) totally failed to describe the behavior of G-V curves at higher Ca^{2+}.

of voltage sensors do not appear to be precisely described. The large confidence limits for Vh_c, Vh_o, and L(0) reflect the fact that these parameters tend to be correlated and relatively large changes in one parameter can be compensated for by changes in another parameter. However, for a variety of assumptions about the values of L(0), Vh_c and Vh_o, the estimates of affinity for Ca^{2+} of the low affinity site was consistently near 2.3 mM when the channel is closed and ~0.66 mM when the channel is open. The difference in affinities for the low affinity site is quite a bit smaller than that observed for the high affinity Ca^{2+} sites, defined by K_c and K_o. However, these values for $K(l)_o$ and $K(l)_c$ suggest that the low affinity site, should this model be correct, may contribute substantially to the position of the G-V curve over the range of Ca^{2+} from 100 μM to 1 mM.

We next examined the ability of Eq. 4 to describe the G-V curves obtained with 0 Ca^{2+} with varying Mg^{2+} (data set 2). The resulting fit is shown graphically in Fig. 14 B with values listed in Table I (column B). For fitting the 0 Ca^{2+} plus Δ[Mg^{2+}] G-V curves, values for K_o and K_c were constrained to those obtained when fitting the data over all [Ca^{2+}], since in the absence of Ca^{2+}, these parameters are not defined. Furthermore, we constrained the value of L(0) to that used in column A. This gave an adequate fit to the data, with $K(l)_o$ of ~6.0 mM and $K(l)_c$ of 22.1 mM. When the 0 Ca^{2+} plus various [Mg^{2+}] curves from data set 4 were similarly fit, the resulting estimates of $K(l)_o$ and $K(l)_c$ were 5.7 ± 0.3 and 24.4 ± 1.5 mM, respectively. Thus, binding of Mg^{2+} to the low affinity site appears to be about seven to eight times weaker than binding of Ca^{2+}.

Guided by the analysis of Shi and Cui (2001b), we have extended Eq. 4 to include terms for both the differential affinities of Ca^{2+} and Mg^{2+} for the low affinity site and for the inhibitory action of Mg^{2+} on the high

TABLE I

Parameter Estimates from Fitting Scheme I to GV Curves Generated under Various Conditions

		(A) ΔCa^{2+}	(B) ΔMg^{2+} alone	(C) 300 μM Ca^{2+} + ΔMg^{2+}	(D) 0, 300 μM Ca^{2+} + ΔMg^{2+}	(E) 0, 300 μM Ca^{2+} + ΔMg^{2+}
					$K(h,mg)_c = K(h,mg)_o$	$K(h,mg)_c ! = K(h,mg)_o$
	Units	Data set 1	Data set 2	Data set 3	Data set 4	Data set 4
$K(h,ca)_c$	μM	11.2 ± 0.48	11.2[a]	11.2[a]	11.2[a]	11.2[a]
$K(h,ca)_o$	μM	1.28 ± 0.05	1.3[a]	1.3[a]	1.3[a]	1.28[a]
Vhc	mV	41.8 ± 21.3	41.8[a]	41.8[a]	41.8[a]	41.8[a]
Vho	mV	−125 ± 12.4	−125[a]	−125[a]	−125[a]	−125[a]
z		0.28e[a]	0.28[a]	0.28[a]	0.28[a]	0.28[a]
Q		0. 86 ± 0.04e	0.96 ± 0.07	0.89 ± 0.01	0.93 ± 0.01	0.97 ± 0.01
L(0)		500,000[a]	500,000[a]	500,000[a]	500,000[a]	500,000[a]
$K(l,mg)_c$	mM	—	22.13 ± 1.28	8.46 ± 1.60	14.1 ± 1.04	19.59 ± 1.35
$K(l,mg)_o$	mM	—	5.96 ± 0.27	2.05 ± 0.20	3.46 ± 0.19	3.24 ± 0.15
$K(l,ca)_c$	mM	2.33 ± 0.12	—	2.329[a]	2.321[a]	2.321[a]
$K(l,ca)_o$	mM	0.66 ± 0.035	—	6.62[a]	0.661[a]	0.661[a]
$K(h,mg)_c$	mM	—	—	9.31 ± 30.46	8.24 ± 1.17	3.26 ± 0.41
$K(h,mg)_o$	mM	—	—	5.90 ± 23.60	—	4.73 ± 0.40
SSQ/pt		6.34	5.88	6.82	20.5	17.87

Data set 1: $[Ca^{2+}]$ from 0, 1, 4, 10, 30, 60, 100, 300 mM and 1, 2, 5, 10, 20, 50 and 100 mM. Data set 2: 0 Ca^{2+} plus 0, 0.5, 1, 2, 5, 10, 20, 50, and 100 mM Mg^{2+}. Data set 3: 300 mM Ca^{2+} plus 0, 1, 2, 5, 10, 20, 50, and 100 mM Mg^{2+}. Data set 4: 0 and 300 mM Ca^{2+} plus 0, 1, 5, 10, 50, and 100 mM Mg^{2+}. $K(h)_c$ and $K(h)_o$ correspond to high affinity binding constants for closed and open states, respectively, with ca and mg reflecting the affinities for Ca^{2+} and Mg^{2+}, respectively. $K(l)_c$ and $K(l)_o$ correspond to low affinity binding constants for closed and open states, respectively, with ca and mg reflecting the affinities for Ca^{2+} and Mg^{2+}, respectively.

[a]Parameter was fixed to value indicated.

affinity site. From Eq. 5 of Shi and Cui (2001b) and our Eq. 4, an equation defining the fractional conductance as a function of voltage, $[Ca^{2+}]$, and $[Mg^{2+}]$, reflecting the differential affinities of both divalent cations to each binding site is obtained:

$$G(V,Ca,D) = \frac{1}{1 + B_h B_l \left[\frac{(1 + e^{ZF(V - Vh_c)/RT})}{(1 + e^{ZF(V - Vh_o)/RT})}\right]^4 L(0) e^{\frac{QFV}{RT}}}, \quad (5)$$

where

$$B_h = \left(\frac{1 + [Ca]/K(h,ca)_c + [Mg]/K(h,mg)_o}{1 + [Ca]/K(h,ca)_o + [Mg]/K(h,mg)_o}\right)^4 \quad (6)$$

and

$$B_l = \left(\frac{1 + [Ca]/K(l,ca)_c + [Mg]/K(l,mg)_c}{1 + [Ca]/K(l,ca)_o + [Mg]/K(l,mg)_o}\right)^4. \quad (7)$$

This system is defined by four separate binding affinities for both Ca^{2+} and Mg^{2+}, reflecting binding of each divalent cation to either the open or closed states (subscripts o and c) or to the low or high affinity sites (K(l), K(h)). Term, B_h, and Eq. 6 is equivalent to that used by Shi and Cui (2001b) to describe competition between Mg^{2+} and Ca^{2+} for the higher affinity site, whereas B_l arises from the same considerations applied to the lower affinity site. The relative ability of a cation to act as an activator or inhibitor depends on the ratio of the relative affinities of a particular cation for the closed state compared with the open state. As proposed by Shi and Cui (2001b), at the high affinity site $K(h,mg)_c = K(h,mg)_o$ so that occupancy of the high affinity site by Mg^{2+} simply inhibits the ability of Ca^{2+} to activate the channel.

Therefore Eq. 5 provides a tool to evaluate the adequacy of Scheme I in the presence of potentially competing species of divalent cations. Therefore, we used Eq. 5 to fit G-V curves obtained with 300 μM Ca^{2+} and varying $[Mg^{2+}]$. Using values defined above for the high affinity Ca^{2+} binding, the result of fitting Eq. 5 to the G-V curves with 300 μM Ca^{2+} is shown in Fig. 14 C. Again, values for Eq. 5 can be found that fit the G-V curves reasonably well (Table I, column D) even when most parameters are constrained to values obtained for the Ca^{2+} data set. However, estimates for $K(l,mg)_c$ and $K(l,mg)_o$ differ from those in Table I (column B), possibly because of the limited data set being used to define four different Mg^{2+} affinities. Therefore, we also fit data set 4 in which mM Mg^{2+} was added to either 0- or 300-μM Ca^{2+} solutions in the same set of patches. This yielded the values in Table I, column E, for the assumption that $K(h,mg)_c = K(h,mg)_o$ and column F for the assumption that $K(h,mg)_c ! = K(h,mg)_o$. Although the latter assumption improves the fit, these data sets are probably not robust enough to define such parameters well.

We next used Eq. 5 to fit all G-V values in data sets 1–3 or data sets 1 and 4 simultaneously. In this case, we

TABLE II

Parameter Estimates from Simultaneous Fitting of Data Sets Generated under Different Conditions

Fitting assumption		(A) $K(h,mg)_c! = K(h,mg)_o$	(B) $K(h,mg)_c = K(h,mg)_o$	(C) No Mg^{2+} high affinity binding	(D) $K(h,mg)_c! = K(h,mg)_o$	(E) $K(h,mg)_c = K(h,mg)_o$	(F) No Mg^{2+} high affinity binding
	Units	Data set 1–3	Data set 1–3	Data set 1–3	Data set 1,4	Data set 1,4	Data set 1,4
$K(h,ca)_c$	μM	12.45 ± 0.49	14.15 ± 0.57	13.37 ± 0.53	12.49 ± 0.64	12.83 ± 0.64	11.02 ± 0.61
$K(h,ca)_o$	μM	1.42 ± 0.04	1.46 ± 0.043	1.42 ± 0.043	1.42 ± 0.05	1.42 ± 0.05	1.34 ± 0.06
Vhc	mV	41.8[a]	41.8[a]	41.8 [a]	41.8[a]	41.8[a]	41.8[a]
Vho	mV	−125[a]	−125[a]	−125[a]	−125[a]	−125[a]	−125[a]
z		0.28[a]	0.28[a]	0.28[a]	0.28[a]	0.28[a]	0.28[a]
Q		0.91 ± 0.0048	0.89 ± 0.005	0.89 ± 0.005	0.92 ± 0.007	0.91 ± 0.01	0.92 ± 0.01
L(0)		500,000[a]	500,000[a]	500000[a]	500,000[a]	500,000[a]	500,000[a]
$K(l,mg)_c$	mM	18.5 ± 0.76	11.14 ± 0.61	9.71 ± 0.50	16.85 ± 1.07	14.17 ± 0.91	10.39 ± 0.71
$K(l,mg)_o$	mM	3.00 ± 0.101	3.19 ± 0.14	2.92 ± 0.13	3.28 ± 0.16	3.45 ± 0.170	2.88 ± 0.17
$K(l,ca)_c$	mM	2.5 ± 0.14	3.05 ± 0.19	2.80 ± 0.17	2.50 ± 0.17	2.61 ± 0.18	2.100 ± 0.14
$K(l,ca)_o$	mM	0.68 ± 0.04	0.919 ± 0.059	0.82 ± 0.048	0.67 ± 0.051	0.73 ± 0.053	0.535 ± 0.14
$K(h,mg)_c$	mM	4.16 ± 0.32	22.14 ± 3.95	—	4.42 ± 0.601	7.35 ± 0.76	—
$K(h,mg)_o$	mM	7.00 ± 0.40	—	—	5.43 ± 0.52	—	—
SSQ	8606/1032 pts 8.34	11078/1032 pts 10.37	11476/1032 pts 11.12	11536 /885 pts 13.04	12359/885 pts 13.96	14893/885 pts 16.83	8606/1032 pts 8.34

[a]Parameter was fixed to value indicated.

left the binding affinities for both low and high affinity sites unconstrained during the fitting procedure. The result of a simultaneous fit of data sets 1–3 is shown in Fig. 14 D with values given in Table II, column B. Although individual curves are not as well-described as in Fig. 14 (A–C), the general features of the dependence of the G-V curves on Mg^{2+} and Ca^{2+} are retained. Similar values were also obtained from a simultaneous fit to data sets 1 and 4 (Table II, column D). Table II also lists the fits to the various data sets with differing assumptions about affinity of Mg^{2+} to the high affinity sites, including the absence of Mg^{2+} binding to those sites. Although adequate fits can be obtained when it is assumed that Mg^{2+} does not bind to the high affinity sites, it is clear that such an assumption fails to describe the rightward shift of G-V curves that occurs at 100 mM Mg^{2+} in the presence of 300 μM Ca^{2+}.

On balance, examination of the values in Table II suggest that, despite some variation, the two sets of data (data sets 1–3, and data sets 1 and 4) yield quite comparable estimates for various binding affinities. The results indicate that Ca^{2+} affinity to the low affinity site is approximately seven- to eightfold greater than the Mg^{2+} affinity. The intrinsic allosteric effectiveness (K_c/K_o) of Mg^{2+} for the low affinity site may be somewhat greater than that of Ca^{2+}. However, when data sets with either Ca^{2+} alone or Mg^{2+} alone are compared, the allosteric effectiveness of either Ca^{2+} or Mg^{2+} at the high affinity site appears similar. It is possible that other effects of the very high divalent cation concentrations used here may impact somewhat on the reliability of these estimates. Finally, Mg^{2+} appears to inhibit the high affinity site, with a K_d of ~7–20 mM. Thus, on balance, the particular formulation of the 250-state model given in Eqs. 4 and 5 provides a quite good description of the effects of high concentrations of Ca^{2+} or Mg^{2+} on the steady-state G-V curves of *Slo1* currents, with the binding of Ca^{2+} being approximately seven- to eightfold stronger than that of Mg^{2+}.

The values in Table I exhibit some deviations in some parameters from those estimated in earlier studies (Cox and Aldrich, 2000; Zeng et al., 2001). Although some variation is expected simply because of variability in the positions of G-V curves along the voltage-axes among different sets of data, the values of Z and Q seem a bit surprising. We refit the G-Vs obtained with different Ca^{2+} solutions using only data obtained with [Ca^{2+}] of 300 μM and lower using Eq. 3 to determine to what extent the use of Eqs. 3 or 4 might have impacted on the parameter estimates. These values are given in column E of Table III. In this case, values for Q and Z fall much closer to those obtained by Cox and Aldrich (2000; given in column F), which were guided by estimates from Horrigan for voltage-dependent parameters obtained from activation of *Slo1* currents at 0 Ca^{2+} (Horrigan and Aldrich, 1999; Horrigan et al., 1999). Some of the variation in estimates of Z and Q among different studies most certainly results from the simple process of averaging G-V curves, such that variation among individual G-V curves among patches will result in averaged curves with lessened voltage dependence. In addition, to evaluate the significance of the rather large value for Q and smaller value for Z obtained through the use of Eqs. 4 and 5, we refit the G-V curves obtained over all Ca^{2+} (data set 1) while constraining the values for Q and Z to those used by Cox and Aldrich (2000). This resulted in estimates of $K(l,ca)_o$ and $K(l,ca)_c$ for Ca^{2+} similar to those already given, although values for L(0), Vh_c,

TABLE III

Allosteric Regulation of Voltage-sensor Equilibria Is Unlikely to Account for the Dependence of Slo1 G-V Curves on Millimolar Ca^{2+} or Mg^{2+}

	Units	(A) Ca^{2+} alone: unconstrained[a]	(B) $\Delta[Mg^{2+}]$; 0 Ca^{2+}	(C) $\Delta[Mg^{2+}]$; 0 Ca^{2+}	(D)300 μM Ca^{2+} + $\Delta[Mg^{2+}]$	(E) Eq. 3 for 0–300 μM Ca^{2+}	(F) Cox and Aldrich
K_c	μM	12.22 ± 0.77	12.22[a]	12.22[a]	12.22[a]	1.42 ± 0.11	7.42
K_o	μM	1.35 ± 0.10	1.35[a]	1.35[a]	1.35[a]	15.95 ± 1.05	0.80
Vh_c	mV	87.1 ± 12.0	87.1[a]	3363.3[a]	87.1[a]	156.6 ± 87.1	141.8
Vh_o	mV	−29.9 ± 41.7	−29.9[a]	221.7 ± 663.4	−29.9[a]	−97.4 ± 139.4	−1.0
Z		0.38 ± 0.05e	0.38e[a]	0.38e[a]	0.38 ± 0.01e	0.35 ± 0.05e	0.51e
Q		0.69 ± 0.05e	0.69e[a]	0.69e[a]	0.69 ± 0.04e	0.38 ± 1.17e	0.40e
L(0)		$9.8 \times 10^4 \pm 2.4 \times 10^5$	65,000[a]	499.1 ± 8415	98,242[a]	2.785×10^6	2.91×10^5
K_m	mM	7.3 ± 2.0	18.0 ± 19.6	24.6 ± 113	11.48 ± 0.530	—	—
E		2.15 ± 0.23	2.148[a]	2.148[a]	1.99 ± 0.01	—	—

(A) All values were unconstrained. (B) All values except those for Mg^{2+} action were constrained to those in Column A, except that L(0) was adjusted to allow the curve at 0 Ca^{2+} to be well described. No values could be found for K_m and E that allowed eq. 8 to describe the effects of Mg^{2+} at low Ca^{2+}. (C) A decent fit at low Ca^{2+} could be obtained, but values for L(0), Vh_c and Vh_o differ drastically from those required to describe the effects of Ca^{2+} and Mg^{2+} in A, B, and D. (D) Effects of Mg^{2+} with 300 μM Ca^{2+} can be described by the results obtained with Ca^{2+} alone. (E) Eq. 3 was used to fit G-V curves obtained from 0 Ca^{2+} to 300 μM Ca^{2+}. (F) Values are from Cox and Aldrich (2000).

[a]Parameter was fixed to value indicated.

and Vh_o were altered. On balance, the overall quality of the fits were only somewhat poorer. This analysis would suggest that values for L(0), Vh_c, Vh_o, Q and Z are not well-constrained by this procedure, presumably because of correlations between parameters. However, values for Ca^{2+} and Mg^{2+} affinities appear to be critical for obtaining acceptable fits.

Scheme I Adequately Describes the Effects of Millimolar Ca^{2+} and Mg^{2+}

We next examined the extent to which Scheme I and Eqs. 4 and 5 might account for other aspects of the data. To accomplish this, families of G-V curves predicted by Scheme I with values given in Table II, Column D were subjected to analysis similar to that employed on actual *Slo1* currents. The predictions from Scheme I are overlaid over various experimentally measured values in Fig. 5. In Fig. 5 A, the predicted shift in $V_{0.5}$ caused by different $[Mg^{2+}]$ is plotted over the actual data points for both data sets 3 and 4. The idealized curve was generated assuming Ca^{2+} of 300 μM with the indicated $[Mg^{2+}]$. In Fig. 5 (B and C), the prediction for shifts produced by 10 mM Mg^{2+} at different $[Ca^{2+}]$ are compared with actual data. Scheme I, when the inhibitory action of Mg^{2+} on the high affinity site is included, does an excellent job (Fig. 5 C) of explaining the reduction in shift in $V_{0.5}$ seen at both 4 and 10 μM Ca^{2+}, which is consistent with the observations of Shi and Cui (2001b). Fig. 5 C also shows the expectations for the shift in $V_{0.5}$, when Mg^{2+} binding to the inhibitory site is not assumed. One of the compelling aspects of Fig. 5C is that G-V curves obtained with 4 and 10 μM Ca^{2+} with and without Mg^{2+} were not used in the fitting process we have employed. Yet, the inhibition by Mg^{2+} that is observed with 300 μM Ca^{2+} and more elevated Mg^{2+} does allow a reasonable prediction of the inhibitory effects of 10 mM Mg^{2+} observed at 4 and 10 μM Ca^{2+}. Finally, in Fig. 5 D, the predictions for Scheme I for the relationship between $V_{0.5}$ as a function of Ca^{2+} are compared with actual data. Similarly, the prediction for the behavior of $V_{0.5}$ resulting from channels containing only the high affinity binding sites is compared with the data corrected for the low affinity affect of Mg^{2+}. The correspondence is quite good, with the differences in the latter case arising from the simple fact the Mg^{2+} correction does not take into account an ~17-mV shift caused by 300 μM Ca^{2+} acting at the low affinity site.

Given that Ca^{2+} is likely to be acting at both low and high affinity binding sites to regulate BK gating it is natural to ask how much effect will binding to the low affinity sites have at various Ca^{2+} concentrations. From examination of the expectations of Scheme I for $V_{0.5}$ arising from the high affinity sites alone and for $V_{0.5}$ arising from both sites, the amount of $V_{0.5}$ shift resulting from action on the low affinity sites can be determined. For 10, 30, 60, 100, 300 μM and 1 mM, the expected negative shifts in $V_{0.5}$ resulting from the high affinity site predicted by Scheme I (Table II, column D) are 0.83, 2.4, 4.5, 7.3, 18.6, and 41.6 mV, respectively. Thus, in cases where local Ca^{2+} may rise towards 100 μM, the low affinity site will contribute appreciably to regulation of BK current.

Scheme I Can Account for Unusual Aspects of the Behavior of Hill Coefficients

Another unusual aspect of our observations with high $[Ca^{2+}]$ or with high $[Mg^{2+}]$ were the properties of Hill coefficients and apparent K_d for Ca^{2+} action as a function of voltage. Therefore, from idealized G-V curves generated from the values of Table II, column D, we generated

plots of the activation of conductance as a function of Ca^{2+}. From these, the values for Hill coefficient and K_d were obtained, following the same procedure used for our experimental results. The Hill plots for the Scheme I predictions are given in Fig. 12 B, and the resulting values for K_d and Hill coefficient are overlaid over the actual data in Fig. 12 (C and D, respectively), showing a strong correspondence. The behavior of the Hill coefficient predicted by Scheme I is particularly remarkable, exhibiting a complex voltage dependence that mirrors that determined from the actual data set. The deviations that are observed are probably inconsequential given that so many factors discussed earlier can contribute to unreliability in the Hill coefficient estimates.

We next turned to expectations of Scheme I for the effects of Mg^{2+} on the Hill coefficient using G-V curves generated from values in Table II, column D. From Hill plots obtained for Scheme I predicted G-V curves, estimates of K_d and Hill coefficient with and without Mg^{2+} are plotted in Fig. 13 (E and F, respectively), for both the assumption of Mg^{2+} inhibition of the high affinity site and lack of inhibition. As just shown, the apparent affinity is increased with depolarization, with Mg^{2+} producing an increase in apparent affinity at all voltages (Fig. 13 E). A segment of the Scheme I predictions are also overlaid over the data in Fig. 13 C showing the correspondence between data and model. In this case, we refit the simulated Hill plots using only values for 1 μM to 1 mM Ca^{2+}, with and without addition of 10 mM Mg^{2+}. As shown, Scheme I predicts that Mg^{2+} will increase the apparent Hill coefficient over the range of voltages (0-50 mV) that have typically been examined in previous studies (Golowasch et al., 1986; Oberhauser et al., 1988). However, above +50 mV the values in the presence and absence of Mg^{2+} converge, although this is a range that is difficult to study experimentally with added Mg^{2+}. The essential point is that Scheme I does predict that Mg^{2+} should cause an increase in apparent Hill coefficient, although it should be kept in mind that this effect has nothing to with numbers of Ca^{2+} binding sites per se. Predictions for the Hill coefficients were also generated for Scheme I, but for the case in which the Mg^{2+} inhibitory effect on the high affinity site does not occur. The expectations for the Hill coefficients are largely unchanged, indicating that Mg^{2+} block per se does not contribute to the Mg^{2+} dependence of the Hill plots, but rather that the Hill plots are a reflection of the existence of multiple divalent cation regulatory sites with differing affinities. Thus, for this channel, the activation of conductance is a complex function of multiple kinds of divalent cation binding sites with differing affinities, such that a Hill plot may not be mechanistically informative tool for analysis of this channel.

Coupling of Mg^{2+} Binding to Voltage-sensor Equilibria Is Unlikely to Account for the Results

Although Scheme I seems to provide a quite compelling description of the behavior of *Slo1* currents over a variety of conditions, it should be kept in mind that alternative assumptions for a 250-state model can also be made. Therefore, we considered the possibility that the low affinity divalent cation site may somehow be coupled to the equilibria of the voltage-sensor movement (V_o or V_c), such that, dependent on the extent of ligation by Mg^{2+}, the voltage-sensor equilibrium would now be defined by $V_{o(0)}$–$V_{o(4)}$, and $V_{c(0)}$–$V_{c(4)}$. This is given in Scheme II.

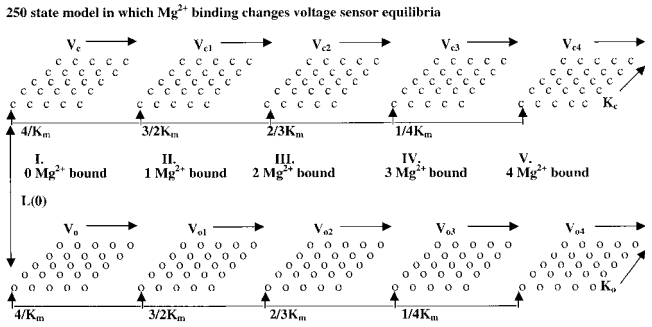

(SCHEME II)

The resulting set of equations therefore contains terms for K_m, the affinity of Mg^{2+} binding, and terms for voltage-sensor movement just given. We then assumed that the binding of each Mg^{2+} alters the voltage-sensor equilibria by an allosteric factor, E, such that $V_{c(1)} = EV_{c(0)}$, $V_{c(2)} = E^2V_{c(0)}$, and so on. This assumption which has parallels in the analysis of Horrigan regarding coupling of voltage-sensor movement and channel opening (Horrigan and Aldrich, 1999) results in two additional free parameters, E and K_m over the terms introduced in Eq. 3 (Cox and Aldrich, 2000). However, the resulting equation is considerably more complex than that given in Eq. 4. Specifically,

$$P(V,Ca,D) = \frac{1 + 4\frac{[D]}{K_m}M_1 + 6\left(\frac{[D]}{K_m}\right)^2 M_2 + 4\left(\frac{[D]}{K_m}\right)^3 M_3 + \left(\frac{[D]}{K_m}\right)^4 M_4}{1 + BL\left[N_0 + 4\frac{[D]}{K_m}N_1 + 6\left(\frac{[D]}{K_m}\right)^2 N_2 + 4\left(\frac{[D]}{K_m}\right)^3 N_3 + \left(\frac{[D]}{K_m}\right)^4 N_4\right]}, \quad (8)$$

where for i = 1–4

$$B = \left[\frac{1 + [Ca]/K_c}{1 + [Ca]/K_o}\right]^4,$$

$$M_i = \frac{1 + E^i e^{ZF(V - Vh_o)/RT}}{1 + e^{ZF(V - Vh_o)/RT}}$$

and for i = 0–4,

$$N_i = \frac{1 + E^i e^{ZF(V - Vh_c)/RT}}{1 + e^{ZF(V - Vh_o)/RT}}.$$

L, K_c, K_o, Vh_c, and Vh_o, Z, and Q are identical to their meanings given above. As expected, when [D] is 0 or K_m is exceedingly high, Eq. 8 is reduced to Eq. 3. The fit of Eq. 8 to the G-V curves obtained over all Ca^{2+} is given in Fig. 14 E with values given in Table III (column A), whereas the fit to G-V curves obtained with 0 Ca^{2+} and various [Mg^{2+}] is given in Fig. 14 F with values in Table III (columns B and C). Although Eq. 8 actually yielded a smaller sums of squares to the G-V curves obtained over all Ca^{2+} than Eq. 4, when the values obtained for fitting G-V curves over all Ca^{2+} were used to fit the results at 0 Ca^{2+}, Eq. 8 was not successful in yielding values that could adequately describe the effects of Mg^{2+} at 0 Ca^{2+}. Thus, for the two different data sets, Eq. 8 yielded entirely different parameter estimates, indicating that some assumption made in Scheme II and Eq. 8 does not account for the behavior of *Slo1* currents.

However, when the allosteric factor E in the above equations was altered so that its value was somewhat greater for open channels than for closed channels, it was possible to obtain values that could describe the behavior at low Ca^{2+}. This adjustment in effect creates an extra free parameter beyond that used in Eq. 4. Furthermore, if the voltage-sensor equilibrium is affected differently by Mg^{2+} when the channel is open or closed, this implicitly requires that Mg^{2+} affinity be different in the two cases, analogous to the case we previously considered. Thus, a model in which binding of each Mg^{2+} alters the voltage-sensor equilibrium by a constant allosteric factor appears inadequate to account for the present results. It should be kept in mind that the present use of a Mg^{2+}-dependent allosteric factor is only one way that Mg^{2+} binding might be related to the voltage sensor equilibrium. However, we have also considered the case that binding of each Mg^{2+} results in a fixed shift (ΔV) for either Vh_c or Vh_o. Analysis of this case yielded results similar to that obtained assuming an allosteric factor, E.

Accounting for the Kinetic Effects of Mg^{2+}

Although Scheme I provides a reasonable description of the effects of high concentration of Mg^{2+} and both low and high concentrations of Ca^{2+} on *Slo1* G-V curves, Mg^{2+} and Ca^{2+} have distinct differences in their effects on channel kinetics. Specifically, Mg^{2+} does not increase current activation rates (except at very high concentrations) but slows current deactivation. In contrast, Ca^{2+} at μM concentrations increases current activation rates at strong activation voltages, while also slowing current deactivation over a broad range of concentrations. These effects were summarized in Fig. 11. Given the assumptions in Scheme I, these differences might seem surprising. Both the high affinity binding site for Ca^{2+} and the lower affinity nonselective site are proposed to simply alter L(0), the equilibrium constant between closed and open channels at 0 mV imposed voltage. The low affinity site does not alter the high affinity binding constants and vice versa. Thus, one might expect that both Ca^{2+} acting on the high affinity site or Mg^{2+} acting on the low affinity site might result in similar effects. However, these differences can simply be explained if the high and low affinity sites differentially affect the rates of transition between closed and open states that determine L(0). Specifically, if the high affinity site primarily enhances the rate of channel opening, whereas the lower affinity site primarily regulates the rate of closing, both the steady-state G-V curves and the kinetic effects can be explained. To show this, we examined how binding of Mg^{2+} might alter activation and deactivation rates for a *Slo1* channel gating in the absence of any Ca^{2+} assuming rate constants from Horrigan (Horrigan and Aldrich, 1999) and Mg^{2+} binding constants given in Table I. Binding of Mg^{2+} was assumed to alter the closed-open equilibrium without affecting the voltage-dependent transitions. If the coupling of Mg^{2+} to channel opening was entirely assigned to the channel closing rates, this resulted in a slowing of activation and deactivation time constants over all voltages, although at positive activation potentials time constants with and without Mg^{2+} converged. In contrast, if the coupling to the channel opening transitions is reflected in effects on both channel opening and channel closing rates, then both an increase in current activation rate and a slowing of deactivation can be observed, as seen with μM Ca^{2+} concentrations. This implies that the low and high affinity sites, although both allosterically coupled to the closed-open equilibrium, do so in quite distinct ways.

DISCUSSION

The dependence of activation of BK channels on cytosolic [Ca^{2+}] is remarkable in that the dependence of BK channel open probability on voltage is shifted by a range of [Ca^{2+}] that spans over four log orders (~0.8 μM–20 mM). At a single voltage, the dependence of BK channel conductance on [Ca^{2+}] is described by a typical binding isotherm involving a Hill coefficient of ~2. To account for this enormous range of concentrations by which a single ligand can influence channel gating implicitly requires either that Ca^{2+} binding, per se, exhibit voltage dependence (Moczydlowski and Latorre, 1983) or that there exist multiple kinds of Ca^{2+} binding regulatory sites each with somewhat overlapping affinities.

The present results show that at least two types of Ca^{2+} binding sites influence *Slo1* activation. First, there

are sites that bind Ca^{2+} quite specifically with affinities in the micromolar range. Occupation of these relatively high affinity sites typically increases the activation rate of BK channels at a given level of depolarization. Mg^{2+} appears to be a weak competitive inhibitor at these sites (Shi and Cui, 2001b). Second, there are sites that bind Ca^{2+} with affinities in the millimolar range which are able to shift activation of open channels to more negative potentials. Mg^{2+} is able potentiate activation of the channel by binding to more strongly to these low affinity sites when the channel is open, than when it is closed. The data show that binding of divalent cations to the low affinity site has no influence on the rates of channel activation at limiting conditions, but appears to stabilize the channel in open states, thereby slowing current deactivation.

These results provide further support for the view that the voltage- and Ca^{2+}-dependent transitions that lead to *Slo1* activation are separate processes. In the presence of 10 mM Mg^{2+}, Ca^{2+} concentrations above ~100 μM do not result in any additional negative shift in the $V_{0.5}$. Similarly, the rate of activation of *Slo1* current at a particular voltage exhibits saturation above 100 μM Ca^{2+}. Thus, Ca^{2+}-dependent sites important for limiting channel activation appear to be fully occupied at $[Ca^{2+}]$ of 100 μM or so. In the presence of Mg^{2+}, the $V_{0.5}$ is essentially unchanged over a 100-fold increase in $[Ca^{2+}]$ (100 μM to 10 mM). Activation of currents under these conditions, however, remains voltage-dependent. Thus, activation of *Slo1* current clearly results from separate voltage-dependent and Ca^{2+}-dependent activation transitions as argued previously (Cox et al., 1997a; Cui et al., 1997). This conclusion implies that binding of Ca^{2+} to the high affinity sites is saturable. This is consistent with the apparent saturation in current activation rate observed with $[Ca^{2+}]$ ~100 μM (Cui et al., 1997) and with the lack of change in single-channel kinetics at +30 mV over $[Ca^{2+}]$ from 132 to 1,024 μM (Rothberg and Magleby, 1999).

The conclusion that Ca^{2+} and Mg^{2+} share a common low affinity binding site is justified by three results. First, the activation of *Slo1* in the presence of 10 mM Ca^{2+} is remarkably similar to that measured in the presence of 300 μM Ca^{2+} plus 10 mM Mg^{2+}. Second, the effects of very high concentrations of Ca^{2+} and Mg^{2+} on *Slo1* activation do not appear to be additive. Third, the kinetic effects of similar high concentrations of Mg^{2+} and Ca^{2+} are comparable, in terms of their ability to similarly shift $V_{0.5}$, slow deactivation, and have minimal affect on current activation. Together, the results show that the effects of $[Ca^{2+}]$ and $[Mg^{2+}]$ at ≥1 mM result from action at sites distinct from those affected by lower $[Ca^{2+}]$. Once these low affinity sites are taken into account, the results reveal that the key Ca^{2+}-dependent steps leading to channel activation are, in fact, saturable and voltage-independent. However, the present analysis suggests that, although these low affinity sites are relatively nonselective, they do exhibit an approximately seven- to eightfold greater affinity for Ca^{2+} over Mg^{2+}.

What Is the Nature of the Low Affinity Divalent Binding Site

That high concentrations of both Ca^{2+} or Mg^{2+} produce a similar marked shift in BK current activation raises the possibility that the shift may result from the screening of negative surface charges on either the oocyte membrane or on the channel protein itself. The reduction of negative charge on or nearby ion channel proteins by divalent cations can explain negative shifts in activation of some currents (Green and Anderson, 1991; Hille, 1992) and the reduction of single-channel conductance in others (Imoto et al., 1988), including the BK channel (MacKinnon et al., 1989; MacKinnon and Miller, 1989). However, several points argue against a surface-potential mechanism in the present case. First, the magnitude of $V_{0.5}$ shifts caused by Mg^{2+} may be too large to be explained solely on the basis of surface charge screening. According to the Gouy-Chapman model for electrostatic potential due to fixed charges close to a membrane bilayer, divalent cations can change local potentials by a maximum of 29 mV per 10-fold increase in concentration (McLaughlin et al., 1971). Our data show that increasing $[Mg^{2+}]$ from 1 to 10 mM in the presence of 100 μM Ca^{2+} can shift activation by >45 mV. Second, the inability of Mg^{2+} to substantially reduce the single-channel conductance at negative potentials implies that any local field changes associated with high $[Mg^{2+}]$ are minimal. Third, the ability of divalent cations to screen surface charges is known to depend on the ionic strength of the surrounding solution (McLaughlin et al., 1971). The shifts described here were obtained under conditions of relatively high ionic strength, namely 160 mM K^+, which would be expected to minimize any surface potential contributions. Finally, direct evidence for saturation in the effects of Mg^{2+} were presented, arguing that the effect involves a saturable divalent cation binding site. These observations argue against the possibility that simple screening of charges on the oocyte membrane or channel protein can account for the observed shifts in *Slo1* $V_{0.5}$.

Despite the likelihood that the effects of mM Ca^{2+} and Mg^{2+} cannot be accounted for by surface potential effects, the results are probably insufficient to completely exclude the possibility that some component of the shift produced by high $[Ca^{2+}]$ and $[Mg^{2+}]$ might result from other actions of these cations, perhaps involving surface charge screening. One aspect of both sets of data (data sets 3 and 4) obtained with 0 Ca^{2+} and $[Mg^{2+}]$ up through 100 mM was that clear saturation in the shifts in $V_{0.5}$ was not observed (Fig. 14, D2). Our results in this regards appear similar to those of

Shi and Cui (2001b), in that increases of $[Mg^{2+}]$ from 30 to 100 mM continues to shift $V_{0.5}$. In contrast, shifts in $V_{0.5}$ with elevations of $[Ca^{2+}]$ above 10 mM do appear to saturate. Although these differences may, in part, might simply reflect the weaker affinity of Mg^{2+} to the low affinity site, an additional effect of elevated divalents may also be involved. Similarly, the anomalous increase in current activation rate observed at 50 and 100 mM Mg^{2+} might reflect the consequence of a surface potential effect or other action of very elevated $[Mg^{2+}]$.

The Significance of the Hill Coefficient

The ability of Mg^{2+} and other divalent cations to potentiate BK channel activation by Ca^{2+} is associated with an increase in the Hill coefficient for activation by Ca^{2+} (Golowasch et al., 1986; Oberhauser et al., 1988). At +20 to +30 mV, the Hill coefficient for Ca^{2+}-dependent activation rose from an average of 2.0 to ~4.2 upon addition of 10 mM Mg^{2+} (Golowasch et al., 1986). In accordance with the significance of the Hill coefficient in studies of other ligand–effector interactions, such results, although rather perplexing, were interpreted as estimates of the minimum number of Ca^{2+} binding sites on the channel protein. Our results with Ca^{2+} alone, therefore, would appear in general agreement with this earlier work, with an increase in Hill coefficient from ~2 to over 3 over the same voltage range with smaller increases at more negative potentials. However, even in the absence of Mg^{2+}, Hill coefficients as high as 3–4 have been reported in some studies (Cui et al., 1997) at test potentials above +80 mV.

The present analysis suggests that some of the complexity of the behavior of the Hill coefficient for BK channels can be most simply explained by activation models involving the presence of multiple kinds of divalent cation binding sites, with differing affinities. In fact, the unusual aspect of the earlier Hill coefficient estimates may not be the higher estimates (2–3), but rather the lower estimates (0.5–1.0). The lower estimates appear to arise at voltages where the two separate binding affinities may both contribute to the Ca^{2+} dependence of conductance activation. In the presence of Mg^{2+}, the contribution of Ca^{2+} mediated by the low affinity site is removed, such that the higher estimates largely reflect the action of Ca^{2+} at the high affinity sites alone. The complex shape of the behavior of the Hill coefficient predicted from Scheme I in the presence and absence of Mg^{2+} (Fig. 13 F) would seem to lend itself to additional experimentation. Unfortunately, many of the interesting voltages that could be tested are not readily amenable to reliable estimates of channel conductance as a function of $[Ca^{2+}]$.

Allosteric Modulation of Slo1 Current

Gating of BK channels is unusual in that two physiological stimuli, Ca^{2+} and voltage, act in concert to regulate activation of conductance. Even with the initial recording of single BK channels in bilayers (Moczydlowski and Latorre, 1983; Vergara and Latorre, 1983) and in patches from native cells (Pallotta et al., 1981; Barrett et al., 1982), it was apparent that multiple closed and open states were required to account for the behavior of single channels. With higher resolution recording and advances in analysis, the sophistication of these models increased (McManus and Magleby, 1988, 1991). More recently, both from single-channel recording and macroscopic recordings of cloned *Slo1* currents two-tiered 50-state activation models have provided a valuable conceptual way of relating the tetrameric nature of the channel proteins to their functional behavior (Rothberg and Magleby, 1999; Cox and Aldrich, 2000; Rothberg and Magleby, 2000). Such 50-state, two-tiered models arise as the natural consequence of kinetic transitions corresponding to four separate Ca^{2+} binding steps (one to each subunit), to movement of four separate voltage-sensors, and to the channel closed to open conformational change. Dependent on postulated coupling among different kinetic transitions, a variety of 50-state models can be considered. However, Cox and Aldrich found that by making one particular assumption they were able to describe the behavior of *Slo1* G-V curves over a wide range of Ca^{2+} concentrations (Cox and Aldrich, 2000). Specifically, Ca^{2+} binding steps and movement of the voltage sensors were postulated to occur entirely independently. This conclusion has been nicely supported by mutations in the S4 voltage-sensing region, which support the idea that activation energy provided by voltage and Ca^{2+} binding are additive (Cui and Aldrich, 2000). However, both in our earlier work (Wei et al., 1994; Solaro et al., 1995) and the work of others (Cox et al., 1997a), there have been indications that there may be effects of Ca^{2+} at higher concentrations which would not be accounted for by the 50-state models so far considered.

Here, following previous models that take into account the tetrameric nature of the channel protein, we have extended the general 50-state two-tiered model to now include four low affinity divalent cation sites. The consequence of the addition of these four additional sets of tiers is a 250-state model. However, although the number of states in such models may, at first glance, seem unmanageable, the allosteric nature of such schemes allows useful simplying analytic assumptions that in many ways are conceptually much simpler than many sequential schemes involving even an order of magnitude fewer kinetic states. With the addition of Mg^{2+} binding steps, three possible interpretations of the action of Mg^{2+} could be imagined. In one case, Mg^{2+} might in some way

alter the affinity of Ca^{2+} for its binding sites. This possibility was excluded from consideration, since the effects of Mg^{2+} are apparent in the complete absence of Ca^{2+}. Mg^{2+} might also alter the equilibrium of voltage-sensor movement. In the second case, we evaluated two different assumptions about how Mg^{2+} binding might be coupled to movement of voltage-sensor movement. In both cases, parameter estimates that described the results at higher Ca^{2+} concentrations failed to describe the effects of Mg^{2+} at 0 Ca^{2+}. Thus, this category of model fails to describe the results, unless additional assumptions are made. Finally, we showed that a model in which Mg^{2+} binding is not coupled either to Ca^{2+} binding or to voltage-sensor movement does a quite adequate job of describing many facets of the behavior of *Slo1* currents studied with Ca^{2+} and Mg^{2+}.

The presence of both low affinity and high affinity Ca^{2+} binding sites provides a compelling explanation for how Ca^{2+}, over such a wide range of concentrations, can continue to shift $V_{0.5}$. At the highest concentrations, our results show that eventually a limit to the shift in $V_{0.5}$ does occur but not until $[Ca^{2+}]$ in excess of 20 mM. Yet, the two binding sites postulated here allow a remarkably linear shift in $V_{0.5}$ from ~1 μM to 20 mM, a concentration range spanning over four orders of magnitude. As pointed out initially, there are differences among different studies in how $V_{0.5}$ varies with Ca^{2+} over this range. Some studies have revealed quite linear relationships (Meera et al., 1996), while others exhibit marked saturation in the range of 100 μM–1 mM (Wei et al., 1994; Cui et al., 1997). Even in our own experience among different batches of oocytes, the extent to which saturation is observed varies. We consider it possible that there remain unknown factors, perhaps dependent on factors in oocytes, that may separately regulate the affinities of the high affinity sites, $K(h)_c$ and $K(h)_o$, relative to the low affinity sites, $K(l)_c$ and $K(l)_o$. This would easily account for subtle differences in the $V_{0.5}$ versus pCa relationship.

Although the results presented here seem, on balance, remarkably congruent with the predictions of Scheme I, there remain some aspects of the data that will require further investigation. First, we consider it possible that there may be surface potential effects that influence our estimates of the low affinity binding affinities. Second, the ability of Mg^{2+} to produce shifts in $V_{0.5}$ in the presence of 300 μM Ca^{2+} appears to be somewhat less than what Scheme I predicts based on shifts produced with 0 Ca^{2+}. This is true even for data set 4 in which effects of Mg^{2+} on currents activated with either 0 or 300 μM Ca^{2+} were examined in the same set of patches. Third, the apparent increase in current activation rate produced at 50 and 100 mM Mg^{2+} with 0 Ca^{2+} does not seem consistent with the lack of effect of Mg^{2+} on activation rates studied under other conditions.

Despite the uncertainties just mentioned, together, the results of Shi and Cui (2001b) and those presented here provide what seems an essentially complete description of the ability of Mg^{2+} and Ca^{2+} to regulate gating of BK channels. Our estimates for binding affinities of Mg^{2+} to the low affinity site ($K(l,mg)_c \sim 14$–16 mM; $K(l,mg)_o \sim 3$–4 mM) are essentially identical to the values of 15.0 and 3.6 mM obtained by Shi and Cui (2001b), while estimates of the blocking effect of Mg^{2+} on the high affinity binding sites are also comparable. It remains possible that either the high affinity or low affinity effects actually involve mediation by multiple high or low affinity sites, although certainly nothing in the results requires that. Our results indicate that the relative affinities of Ca^{2+} and Mg^{2+} for the low affinity site differ by about a factor of sevenfold. Although among different sets of data, we feel that a two- to threefold difference might result from normal variability seen with *Slo1* currents, we think that the difference in Ca^{2+} and Mg^{2+} affinities for the low affinity site reflects a true selectivity, although rather weak, for Ca^{2+} over Mg^{2+}. Now that the path is clear to how the low affinity site can be studied in isolation, it will be interesting to determine its ionic selectivity more rigorously.

Physiological Regulation by Cytosolic Mg^{2+} or Ca^{2+} Mediated by the Low Affinity Site

The ability of cytosolic $[Mg^{2+}]$ on the order of 1 mM to regulate BK current raises the possibility that this low affinity site and the shift in gating it produces may define a physiologically important mechanism of BK current regulation. The understanding of the mechanisms of regulation and dynamics of cytosolic free Mg^{2+} levels remain limited (Romani and Scarpa, 2000). Based on evidence from a variety of cell types, free Mg^{2+} is thought to be ~0.5–1 mM. Most cytosolic Mg^{2+} will be associated with di- and triphosphate nucleotides, and circumstances that deplete cytosolic ATP are thought to result in transient increases in free $[Mg^{2+}]$ with associated extrusion of Mg^{2+} from cells (for review see Romani and Scarpa, 2000). Thus, published resting free $[Mg^{2+}]$ are likely sufficient to begin to modulate BK channel activity via the low affinity divalent cation site. Dependent on the magnitude of any transient changes in $[Mg^{2+}]$, modulation of BK channel gating could be substantial.

In the case of Ca^{2+}, the affinity of the low affinity binding site for Ca^{2+} is such that Ca^{2+} will begin to influence the behavior of the *Slo1* currents through this site at concentrations ~30 μM. Thus, for those BK channels that are tightly coupled to sites of Ca^{2+} influx, it is likely that occupancy of the low affinity site will occur following channel opening, thereby regulating BK channel function.

Conclusion

These results show that there are at least two types of Ca^{2+} binding sites important for activation of *Slo1* BK channels. First, there are high affinity sites that bind Ca^{2+} relatively specifically which, along with membrane depolarization, influence channel opening rates and activation probability. These sites are likely to be important for activation of BK channels at physiological submembrane Ca^{2+} concentrations and influence the rate of current activation after a voltage-step. A second site (or sites) can bind either Ca^{2+} or Mg^{2+} with a relatively lower affinity, and is able to enhance channel open probability by stabilizing channels in open states, once they have been activated. This results in a shift in G-V curves to more negative voltages. Occupancy of this site does not influence microscopic transitions leading to channel opening, but does slow the rate at which channels leave open states. Thus, regulation of BK channel gating by divalent cations involves multiple types of binding sites with functionally distinct consequences.

We especially thank Jianmin Cui for discussions and J. Shi and J. Cui for sharing their manuscript. The final version of this paper has benefited greatly from their insights into the inhibitory effect of Mg^{2+} on the high affinity Ca^{2+} binding site. We thank Lynn Lavack for injection and care of oocytes and the Zorumski lab for providing oocytes. We also thank Carl Nelson for participation in many experiments during the initial stages of this work.

This work was supported by the National Institutes of Health grant DK46564 (to C. Lingle).

Submitted: 30 July 2001
Revised: 26 September 2001
Accepted: 27 September 2001

REFERENCES

Barrett, J.N., K.L. Magleby, and B.S. Pallotta. 1982. Properties of single calcium-activated potassium channels in cultured rat muscle. *J. Physiol.* 331:211–230.

Bian, S., I. Favre, and E. Moczydlowski. 2001. Ca^{2+}-binding activity of a COOH-terminal fragment of the *Drosophila* BK channel involved in Ca^{2+}-dependent activation. *Proc. Natl. Acad. Sci. USA.* 98:4776–4781.

Braun, A., and L. Sy. 2001. Contribution of potential EF hand motifs to the calcium-dependent gating of a mouse brain large conductance, calcium-sensitive K^+ channel. *J. Physiol.* 533:681–695.

Butler, A., S. Tsunoda, D.P. McCobb, A. Wei, and L. Salkoff. 1993. mSlo, a complex mouse gene encoding "maxi" calcium-activated potassium channels. *Science.* 261:221–224.

Cox, D., and R. Aldrich. 2000. Role of the β1 subunit in large-conductance Ca^{2+}-activated K^+ channel gating energetics. Mechanisms of enhanced Ca^{2+} sensitivity. *J. Gen. Physiol.* 116:411–432.

Cox, D.H., J. Cui, and R.W. Aldrich. 1997a. Allosteric gating of a large conductance Ca-activated K^+ channel. *J. Gen. Physiol.* 110: 257–281.

Cox, D.H., J. Cui, and R.W. Aldrich. 1997b. Separation of gating properties from permeation and block in mslo large conductance Ca-activated K^+ channels. *J. Gen. Physiol.* 109:633–646.

Cui, J., and R.W. Aldrich. 2000. Allosteric linkage between voltage and Ca^{2+}-dependent activation of BK-type mslo1 K^+ channels. *Biochemistry.* 39:15612–15619.

Cui, J., D.H. Cox, and R.W. Aldrich. 1997. Intrinsic voltage dependence and Ca^{2+} regulation of mslo large conductance Ca-activated K^+ channels. *J. Gen. Physiol.* 109:647–673.

Diaz, L., P. Meera, J. Amigo, E. Stefani, O. Alvarez, L. Toro, and R. Latorre. 1998. Role of the S4 segment in a voltage-dependent calcium-sensitive potassium (hSlo) channel. *J Biol Chem* 273:32430–32436.

Ferguson, W.B. 1991. Competitive Mg^{2+} block of a large-conductance, $Ca^{(2+)}$-activated K^+ channel in rat skeletal muscle. Ca^{2+}, Sr^{2+}, and Ni^{2+} also block. *J. Gen. Physiol.* 98:163–181.

Golowasch, J., A. Kirkwood, and C. Miller. 1986. Allosteric effects of Mg^{2+} on the gating of Ca^{2+}-activated K^+ channels from mammalian skeletal muscle. *J. Exp. Biol.* 124:5–13.

Green, W., and O. Anderson. 1991. Surface charges and ion channel function. *Annu. Rev. Physiol.* 53:341–359.

Hamill, O.P., A. Marty, E. Neher, B. Sakmann, and F.J. Sigworth. 1981. Improved patch-clamp techniques for high-resolution current recording from cells and cell-free membrane patches. *Pflügers Arch.* 391:85–100.

Herrington, J., C.R. Solaro, A. Neely, and C.J. Lingle. 1995. The suppression of Ca^{2+}- and voltage-dependent outward K^+ current during mAChR activation in rat adrenal chromaffin cells. *J. Physiol.* 485:297–318.

Hille, B. 1992. Ionic Channels of Excitable Membrane. 2nd ed. Sinauer Associates, Inc., Sunderland, MA. 607 pp.

Horrigan, F.T., and R.W. Aldrich. 1999. Allosteric voltage gating of potassium channels II. Mslo channel gating charge movement in the absence of Ca^{2+}. *J. Gen. Physiol.* 114:305–336.

Horrigan, F.T., J. Cui, and R.W. Aldrich. 1999. Allosteric voltage gating of potassium channels I. Mslo ionic currents in the absence of Ca^{2+}. *J. Gen. Physiol.* 114:277–304.

Imoto, K., C. Busch, B. Sakmann, M. Mishina, T. Konno, J. Nakai, H. Bujo, Y. Mori, K. Fukuda, and S. Numa. 1988. Rings of negatively charged amino acids determine the acetylcholine receptor channel conductance. *Nature.* 335:645–648.

Lingle, C., X.-H. Zeng, J.-P. Ding, and X.-M. Xia. 2001. Inactivation of BK channels mediated by the NH_2 terminus of the β3b auxiliary subunit involves a two-step mechanism: possible separation of binding and blockade. *J. Gen. Physiol.* 117:583–605.

MacKinnon, R., and C. Miller. 1989. Functional modification of a Ca^{2+}-activated K^+ channel by trimethyloxonium. *Biochemistry.* 28: 8087–8092.

MacKinnon, R., R. Latorre, and C. Miller. 1989. Role of surface electrostatics in the operation of a high-conductance Ca^{2+}-activated K^+ channel. *Biochemistry.* 28:8092–8099.

Martell, A., and R. Smith. 1975. Critical Stability Constants Volume 2: Amines. Plenum Press, New York/London. 415 pp.

McLaughlin, S.G., G. Szabo, and G. Eisenman. 1971. Divalent ions and the surface potential of charged phospholipid membranes. *J. Gen. Physiol.* 58:667–687.

McManus, O.B., and K.L. Magleby. 1988. Kinetic states and modes of single large-conductance calcium-activated potassium channels in cultured rat skeletal muscle. *J. Physiol.* 402:79–120.

McManus, O.B., and K.L. Magleby. 1991. Accounting for the $Ca^{(2+)}$-dependent kinetics of single large-conductance $Ca^{(2+)}$-activated K^+ channels in rat skeletal muscle. *J. Physiol.* 443:739–777.

McManus, O.B., L.M. Helms, L. Pallanck, B. Ganetzky, R. Swanson, and R.J. Leonard. 1995. Functional role of the beta subunit of high conductance calcium-activated potassium channels. *Neuron.* 14:645–650.

Meera, P., M. Wallner, Z. Jiang, and L. Toro. 1996. A calcium switch for the functional coupling between alpha (hslo) and beta subunits (Kv,caβ) of maxi K channels. *FEBS Lett.* 385:127–128.

Moczydlowski, E., and R. Latorre. 1983. Gating kinetics of Ca^{2+}-activated K^+ channels from rat muscle incorporated into planar lipid bilayers. Evidence for two voltage- dependent Ca^{2+} binding reactions. *J. Gen. Physiol.* 82:511–542.

Oberhauser, A., O. Alvarez, and R. Latorre. 1988. Activation by divalent cations of a Ca^{2+}-activated K^+ channel from skeletal muscle membrane. *J. Gen. Physiol.* 92:67–86.

Pallotta, B.S., K.L. Magleby, and J.N. Barrett. 1981. Single channel recordings of Ca^{2+}-activated K^+ currents in rat muscle cell culture. *Nature.* 293:471–474.

Romani, A., and A. Scarpa. 2000. Regulation of cellular magnesium. *Frontiers Biosci.* 5:d720–d734.

Rothberg, B.S., and K.L. Magleby. 1999. Gating kinetics of single large-conductance Ca^{2+}-activated K^+ channels in high Ca^{2+} suggest a two-tiered allosteric gating mechanism. *J. Gen. Physiol.* 114: 93–124.

Rothberg, B.S., and K.L. Magleby. 2000. Voltage and Ca^{2+} activation of single large-conductance Ca^{2+}-activated K^+ channels described by a two-tiered allosteric gating mechanism. *J. Gen. Physiol.* 116:75–99.

Schreiber, M., and L. Salkoff. 1997. A novel calcium-sensing domain in the BK channel. *Biophys. J.* 73:1355–1363.

Schreiber, M., A. Yuan, and L. Salkoff. 1999. Transplantable sites confer calcium sensitivity to BK channels. *Nat. Neurosci.* 2:416–421.

Shen, K.Z., A. Lagrutta, N.W. Davies, N.B. Standen, J.P. Adelman, and R.A. North. 1994. Tetraethylammonium block of Slowpoke calcium-activated potassium channels expressed in *Xenopus* oocytes: evidence for tetrameric channel formation. *Pflügers Arch* 426:440–445.

Shi, J., and J. Cui. 2001a. Intracellular Mg^{2+} activated mSlo Ca^{2+}-activated BK channels. *Biophys. J.* 80:221A (*Abstr.*).

Shi, J., and J. Cui. 2001b. Intracellular Mg^{2+} enhances the function of BK-type Ca^{2+} activated K^+ channels. *J. Gen. Physiol.* 589–605.

Solaro, C., C. Nelson, A. Wei, L. Salkoff, and C. Lingle. 1995. Cytoplasmic Mg^{2+} modulates Ca^{2+}-dependent activation of mSlo by binding to a low affinity site on the channel core. *Biophys. J.* 68:A30.

Vergara, C., and R. Latorre. 1983. Kinetics of Ca^{2+}-activated K^+ channels from rabbit muscle incorporated into planar bilayers. Evidence for a Ca^{2+} and Ba^{2+} blockade. *J. Gen. Physiol.* 82:543–568.

Wallner, M., P. Meera, and L. Toro. 1999. Molecular basis of fast inactivation in voltage and Ca^{2+}-activated K^+ channels: a transmembrane beta-subunit homolog. *Proc. Natl. Acad. Sci. USA.* 96: 4137–4142.

Wei, A., C. Solaro, C. Lingle, and L. Salkoff. 1994. Calcium sensitivity of BK-type KCa channels determined by a separable domain. *Neuron.* 13:671–681.

Xia, X.M., J.P. Ding, and C.J. Lingle. 1999. Molecular basis for the inactivation of Ca^{2+}- and voltage-dependent BK channels in adrenal chromaffin cells and rat insulinoma tumor cells. *J. Neurosci.* 19:5255–5264.

Zeng, X.-H., X.-M. Xia, and C.J. Lingle. 2001. Gating properties conferred on BK channels by the β3b auxiliary subunit in the absence of its N- and C-termini. *J. Gen. Physiol.* 117:607–627.